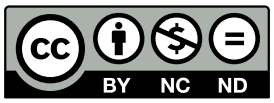

# Ensemble estimation of future rainfall extremes with temperature dependent censored simulation*

David Cross[a,*], Christian Onof[a], Hugo Winter[b]

[a] *Department of Civil and Environmental Engineering, Imperial College London, South Kensington SW7 2AZ, UK*
[b] *EDF Energy R&D UK Centre, Interchange, 81–85 Station Road, Croydon, CR0 2RD, UK*

**Abstract**

We present a new approach for estimating the frequency of sub-hourly rainfall extremes in a warming climate with simulation by conditioning Bartlett-Lewis rectangular pulse (BLRP) rainfall model parameters on the mean monthly near surface air temperature. We use a censored modelling approach with multivariate regression to capture the sensitivity of the full set of BLRP parameter estimators to temperature enabling the parameter estimators to be updated. The downscaling framework incorporates uncertainty in climate model projections for moderate and severe carbon forcing scenarios by using an ensemble of climate model outputs. Linear regression on the logarithm of BLRP parameter estimators offers a robust model for parameter estimation with uncertainty. The approach is tested with 5-minute rainfall data from Bochum in Germany, and Atherstone in the United Kingdom. We find that the approach is highly effective at estimating rainfall extremes in the present climate, and the estimation of future rainfall extremes appears highly plausible.

*Keywords:* mechanistic stochastic, extremes, rainfall, climate change impacts, K nearest neighbour, multivariate regression.

## 1. Introduction

Drainage system design requires the robust estimation of rainfall extremes at fine spatial and temporal scales. For decades, this has been achieved with historical gauge records. However, the growing consensus that anthropogenic climate change is accelerating, challenges the premise that climate stationarity can be assumed over the lifetime of civil infrastructure. This not only impacts new build projects but has direct consequences for existing environments. Increasingly, utility providers are required to assess the resilience of their assets to natural hazards, while businesses and individuals alike seek greater insurance against perils not previously perceived.

Our principal tools for projecting future climate feedbacks are global circulation (GCM) and earth system (ESM) models. However, the coarse resolution of these models makes their outputs unsuitable for climate impact assessment at the urban scale (Burlando and Rosso, 1991; Sunyer et al., 2012). Downscaling techniques are therefore required to quantify the effect of global scale warming on catchment processes. Numerous methods exist including resampling (Thorndahl et al., 2017), scaling (Lenderink and Attema,



*Corresponding author
*Email address:* dmacross@yahoo.com (David Cross)

2015), method of fragments (Srikanthan and McMahon, 2001), disaggregation (Hay et al., 1992; Gyasi-Agyei, 2011), adjusting procedures (Koutsoyiannis and Onof, 2001; Yusop et al., 2014; Abdellatif et al., 2013; Debele et al., 2007), and multifractal cascade models (Schmitt, 2014; Verrier et al., 2011). However, a popular approach is to use stochastic weather generators to synthesise long sequences of environmental variables at the catchment scale, with perturbed parameters to reflect future changes at the climate scale. These can be used to estimate changes to important properties such as variance and extremes, or as inputs into hydrological models to investigate catchment response. Significant progress has been made in this respect since the early 1990s and is described in numerous reviews and comparison articles (Fowler et al., 2007; Sunyer and Madsen, 2009; Maraun et al., 2010b; Arnbjerg-Nielsen, 2011; Sunyer et al., 2012; Willems et al., 2012; Ailliot et al., 2014; Westra et al., 2014; Sunyer et al., 2015).

The purpose of this research is to investigate if temperature projections from an ensemble of CMIP5 global climate models can be used to downscale 5-minute rainfall extremes using stochastic simulation. While there are many other environmental indicators of rainfall, temperature is chosen based on its known high correlation with rainfall and the relatively high skill of climate models in estimating temperature compared with other variables. Furthermore, several studies have investigated the relative importance of different environmental variables as indicators of rainfall, with many concluding that temperature is a key indicator.

The Bartlett-Lewis rectangular pulse (BLRP) model is chosen to enhance the physical basis of extreme rainfall estimation in a changing climate. Mechanistic-stochastic rainfall models such as the BLRP model emulate the theory of rain cell clustering in storms. Consequently, extremes are constructed from the superposition of rain cells making this class of model particularly appealing for extreme rainfall estimation. Taking the censored rainfall modelling approach introduced in Cross et al. (2018), in which BLRP rainfall models are used to simulate the intense rainfall profile over a low censor, we further develop the fitting methodology to allow for climate non-stationarity. Motivated by the simple linear regression on summary statistics of Wasko and Sharma (2017), and the change of conditioning variable in Kaczmarska et al. (2015), the censored modelling approach is extended into a downscaling framework. Following Kaczmarska et al. (2015), we change the conditioning variable from calendar month to mean monthly near surface air temperature, but use K nearest neighbour sampling to identify the training data for model parameter estimation.

To enable simulation under hypothesised warming scenarios, we investigate the sensitivity of censored BLRP model parameters to temperature using multivariate linear regression which preserves the known dependence between parameters. The relation between rainfall model parameters and temperature is established with historical observations. Using an ensemble of mean monthly temperature projections from the CMIP5 inter-comparison experiment, we estimate the change in rainfall extremes for the far future time window 2070-2100 under moderate and severe representative concentration pathways, RCP4.5 and 8.5 respectively. Because the perturbation of model parameters is underpinned by a physical atmospheric process, this downscaling approach is preferable to other established methods, in particular change factors.

A review of the principal developments in rainfall downscaling is presented in Sect.2. In Section 3, we set out the downscaling methodology for extreme rainfall simulation with censoring including BLRP model fitting and parameter regression. Rainfall and climate model data are introduced in Sect.4, followed by the calibration and validation of the models in Sect.5. Extreme rainfall estimation for present and future climates is presented in Sect.6. Discussion and conclusions are given in Sects.7 and 8.

## 2. Developments in rainfall downscaling

### *2.1. Established methods*

Early attempts at downscaling climate model outputs for hydrological analysis focussed on weather typing (Bárdossy and Plate, 1992; Goodess and Palutikof, 1998; Trigo and DaCamara, 2000; Fowler et al., 2000; Bárdossy et al., 2002; Qian et al., 2002; Fowler et al., 2005) in which stochastic weather generators are conditioned on homogeneous mesoscale circulation patterns. This approach is attractive because circulation patterns describe the prevailing weather conditions on a given day and provide discrete integrated series of otherwise continuous non-linear processes. However, because weather types are derived from pressure fields alone, they are unlikely to fully capture the influence of thermodynamic effects on rainfall extremes (Maraun

et al., 2010a) which are known to have a significant impact. This approach has lost favour in the recent decade with greater emphasis being placed on factor of change methods.

Factor of change methods, also referred to as delta-change or perturbation methods (Fowler et al., 2007), apply simple scaling to historical summary statistics according to the change in control and future GCM outputs. Change factors (CF) are used to perturb weather generator parameters so that environmental variables may be simulated at the local scale, but which are representative of changed future climates. While they can be applied to any type of weather generator, CFs have been used extensively with those based on the Neyman-Scott rectangular pulse (NSRP) rainfall model following the development of several weather and rainfall simulation software tools including: EARWIG (Kilsby et al., 2007), AWE-GEN (Fatichi et al., 2011), and RainSim Burton et al. (2008).

The Environment Agency Rainfall and Weather Impacts Generator (EARWIG) is a single site daily weather generator developed for the UK Climate Impacts Programme (UKCIP02) by Kilsby et al. (2007). This downscaling tool comprises a two-part stochastic weather generator which first simulates daily rainfall using the NSRP model, and then daily means of temperature, temperature range, vapour pressure, wind speed and sunshine duration using regressions on the rainfall observations. CFs are calculated for the daily mean, variance and skewness of rainfall, and to a logit transformation of the proportion of dry days using UKCIP02 future scenarios (Hulme et al., 2002). The UK Climate Projections were updated in 2009 (UKCP09, Murphy et al., 2009) following publication of the IPCC (Intergovernmental Panel on Climate Change) fourth assessment report (AR4). Correspondingly, the EARWIG methodology was updated to provide climate change simulations with probabilistic projections from an ensemble of regional climate model (RCM) runs. Subsequently referred to as the UKCP09 weather generator (UKCP09-WG), this approach has formed the basis of significant research into catchment scale climate impacts including studies by Manning et al. (2009), Burton et al. (2010), and Honti et al. (2014).

The Advanced Weather Generator (AWE-GEN Fatichi et al., 2011) is a single site hourly weather generator and downscaling tool. It is similar to the UKCP09-WG in structure, although change factors are assigned probability distributions for a range of climate statistics and applied directly to the rainfall statistics used to fit the embedded NSRP model. Numerous climate impact studies have been undertaken using AWE-GEN (Francipane et al., 2015; Liuzzo et al., 2015; Pumo et al., 2017) to generate hourly rainfall time-series for future climates. A two-dimensional simulator (AWE-GEN-2d) was later developed by Peleg et al. (2017) in which the point NSRP model was replaced with the Space-Time Realizations of Areal Precipitation (STREAP) model (Paschalis et al., 2013) for spatiotemporal rainfall simulation. Despite the significant structural and numerical developments in this model, change factors are still used to estimate the future change in weather variables.

RainSim is an hourly spatiotemporal NSRP rainfall field generator developed by Burton et al. (2008) and is closely related to EARWIG and the UKCP09-WG. It has been used in several climate impact studies using novel downscaling methods. Goderniaux et al. (2011) scale NSRP change factors in RainSim proportionally to global temperature changes to investigate transient climate change impacts on groundwater resources. In a two-part publication, Bordoy and Burlando (2014a,b) apply scaling laws to future daily summary statistics perturbed using change factors calculated at the daily scale. The rescaled future summary statistics are used to reparameterise the space-time RainSim NSRP model to simulate future sub-daily rainfall in the Swiss Alps. Sørup et al. (2016) use the space-time RainSim model to investigate the climate change signal for extreme precipitation over a densely urbanized region of north-eastern Denmark for use in urban drainage design.

Further applications of the change factor approach to downscaling can be found in the literature using similar stochastic rainfall models. Khazaei et al. (2012) use the original NSRP model as the basis of a new weather generator for the estimation of minimum and maximum temperatures. Onof and Arnbjerg-Nielsen (2009) use the random parameter Bartlett-Lewis rectangular pulse (BLRP) model with truncated Gamma distribution to downscale RCM aerial rainfall to sub-hourly point estimates using a combination of change factors and disaggregation. Using a semi-Markov chain model of rainfall events, Sørup et al. (2017) apply change factors for system states which categorise events in the historical record.

Change factors have been used extensively in the recent decades for climate downscaling with rainfall simulators because the method is conceptually tractable and computationally simple. However, it relies

on a certain assumptions which are the matter of debate. Primarily, factor of change methods assume that the scaling relationships of rainfall statistics or model parameters are stationary between present and future climates (Bordoy and Burlando, 2014a; Sunyer and Madsen, 2009). This may be appropriate in locations where there is no reason to believe that the mechanisms governing the local climate will alter significantly, although there is no way to test this assumption for hypothesised future climates. Furthermore, the relationship between mesoscale circulation and point precipitation is assumed to be valid (Forsythe et al., 2014), on the basis that the phenomenology of rainfall generation in storms is scale invariant. In each case, there is no physical underpinning for these assumptions because the scaling relationships are not explained by physical processes or parameters.

*2.2. Linking climate to rainfall*

Trenberth et al. (2003) set out the link between global warming and the intensification of rainfall extremes broadly concluding that as the climate warms atmospheric water vapour content will increase leading to more intense downpours. Explained by the Clausius-Clapeyron (C-C) relationship in which water saturation vapour pressure increases with temperature at a rate of $7\%K^{-1}$, several studies have identified similar scaling relationships between high rainfall quantiles and air temperature (Hardwick Jones et al., 2010; Shaw et al., 2011; Utsumi et al., 2011; Fujibe, 2013; Molnar et al., 2015) supporting the hypothesis that rainfall extremes will intensify with increasing global temperatures. Further evidence is provided by Westra et al. (2013) who identify increasing dependence between maximum annual daily precipitation and globally averaged near surface temperature of between 5.9 and 7.7 $\%K^{-1}$ for two-thirds of over 8000 stations globally.

Despite this, local geography and climate feedbacks can dominate the precipitation - temperature scaling. Ali and Mishra (2017) identify negative scaling between surface air temperature and extreme rainfall in India because of the cooling effect of monsoon events. Hardwick Jones et al. (2010) report negative scaling for Australia above 26 °C while Shaw et al. (2011), Fujibe (2013), and Molnar et al. (2015) find for the USA, Japan and Switzerland respectively that scaling rates vary significantly depending on the region, season, temporal scale and rainfall type. Despite the mixed signals for the C-C relationship, it is physically appealing to identify dependence in precipitation at the local scale with exogenous variables at the mesoscale which capture thermodynamic effects. Such an approach has formed the basis of several studies in the recent decade.

Using a modified-Markov model with kernel density estimator for rainfall occurrence and amounts, Mehrotra and Sharma (2010) present a multisite stochastic downscaling framework in which both occurrence and amount models are conditioned on atmospheric variables. The conditioning variables are chosen to capture atmospheric circulation, moisture and short-term rainfall persistence from rain gauge and NCEP reanalysis data. Using climate projections of the exogenous conditioning variables from CISRO Mk3 climate model, the model is used to evaluate changes in rainfall at the daily, seasonal and annual scales between the current and future climates centred on 2070. The modelling framework presented by Mehrotra and Sharma (2010) offers a tool for climate impact assessment on water resources, but urban scale impacts require rainfall simulation at shorter temporal scales. Mechanistic stochastic rainfall models offer this capability, although as already highlighted downscaling with these models has largely focussed on change factor approaches.

Recognising the demand for non-stationary rainfall simulation in a changing climate, and the limited development of transient model frameworks, Evin and Favre (2013) reformulate the original NSRP model to allow the storm arrival process ($\lambda$) to vary with time. With one additional model parameter representing the evolution in storm arrivals ($\epsilon$), the new transient NSRP model has a total of 6 parameters. A potential criticism of this approach is that the non-stationarity captured in the temporal variation in $\lambda$ is only representative of the historical period. With global warming the rate of change may be different and could vary between the different carbon forcing scenarios set out in the IPCC's fifth assessment reports (AR5, the reader is referred to the Synthesis Report by Pachauri et al. (2014) which combines the findings of the three contributing IPCC working groups).

Wasko and Sharma (2017) use linear regression to establish relationships between monthly rainfall summary statistics and mean monthly air temperature to obtain perturbed fitting statistics for the original NSRP model representative of warmer climates. The simplicity of this approach makes it more pragmatic and potentially more informative than that of Evin and Favre (2013) because historical temperature changes

implicit in Evin and Favre (2013) will not necessarily be representative of the future. However, a possible criticism is that by applying linear regression separately to each summary statistic the dependence structure between statistics may be lost.

Taking a different approach to both Evin and Favre (2013) and Wasko and Sharma (2017), Kaczmarska et al. (2015) develop a new method to calibrate the original BLRP model using continuous environmental covariates instead of calendar month. Using a nonparametric form of local linear regression, BLRP model parameters are estimated using monthly rainfall summary statistics coincident with monthly mean environmental variables. The neighbourhood of summary statistics is weighted by a normalised Gaussian distribution over all data points, with a user defined bandwidth specifying the standard deviation of the distribution. With this approach, parameter estimation beyond the range of the conditioning covariate is highly uncertain because all conditioning months fall within the tails of the normal distribution which are down weighted. This limits the usefulness of local regression for climate impact assessment for the most severe climate forcing scenarios, and far future estimation.

## 3. Downscaling methodology

The downscaling methodology set out here extends the censored rainfall modelling approach for the estimation of fine scale extremes introduced in Cross et al. (2018) to assess climate change impacts on intense rainfall. In this paper, Bartlett-Lewis rectangular pulse models are used to mechanistically simulate short duration intense rainfall from which extremes may be estimated. The method was motivated by the desire to improve the physical realism of extreme rainfall estimation for intense cloudburst type events, to supplement frequency techniques and increase the amount of data used for estimation.

Mechanistic stochastic rainfall models, which include both the Bartlett-Lewis and Neyman-Scott varieties, simulate rainfall by emulating the rainfall generating mechanism with Poisson-cluster processes. In this mechanism, rainfall observed on the ground arises from the clustering of rain cells in storms. Storm arrivals are simulated with a primary Poisson process, and rain cell arrivals with a secondary Poisson process. Rain cells are typically assumed to be rectangular in shape describing their intensity and duration, and storms are terminated according to an exponential distribution. The summation of cells forms the unobserved continuous time rainfall which is aggregated to form discrete rainfall time-series at any temporal scale.

Because of the tendency for mechanistic stochastic rainfall models to under estimate rainfall extremes at fine temporal scales, a censored approach was developed to simulate the intense rainfall profile. In this approach, a low censor is applied to the whole rainfall time-series. Observations below the censor are replaced with zero rainfall, and observations above the censor are reduced by the censor amount. Using three variants of the Bartlett-Lewis rectangular pulse model, the approach was applied to two rainfall records in the UK and Germany for 5 and 15 minute accumulations and shown to significantly improve the estimation of extremes.

Sections 3.1 to 3.4 describe the downscaling methodology presented in this paper. To aid understanding of the procedure, a workflow of the steps involved is presented in Fig.1.

### *3.1. Rainfall model calibration*

The first step in the downscaling methodology is to estimate model parameters that are optimal given the monthly near surface air temperature. To this end, we have to select periods within the historical rainfall record which are representative of a given temperature. The standard method for fitting mechanistic rainfall models essentially uses seasonality as the conditioning covariate represented with non-overlapping calendar months. This is analogous to applying uniform weight to all target months in the historical record, where the target month is the calendar month for which the model is being fitted. The result of this is to obtain seasonally varying parameter estimators for each month of the year.

For the downscaling of rainfall extremes in this study, we propose to change the conditioning covariate for censored rainfall models to mean monthly near surface air temperature. For incremental changes in temperature, we select the calibration data by applying uniform weights to months with mean monthly

Figure 1: Flow diagram setting out the workflow for the downscaling framework with censored rainfall simulation. The CMIP5 ensemble nomenclature, r1i1p1 in step 4, refers to the realisation (starting point), initialisation (method), and physics (parameterisation) applied to each climate model used in this study. See Sect.4.2 for further detail on CMIP5 and the rip-nomenclature. Other ensembles may be chosen for downscaling within this framework.

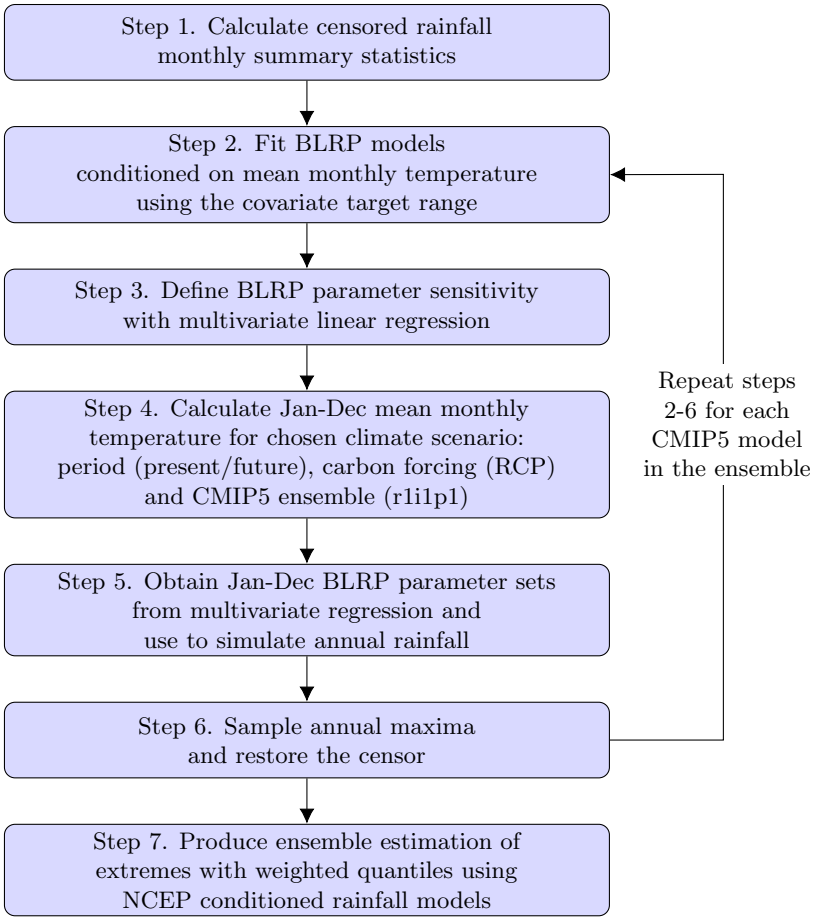


temperatures within a defined bandwidth. In selecting the bandwidth there is a trade-off between making it large enough to ensure optimised parameters are well identified, while keeping it small enough to generate parameter sets which capture the variability of the rainfall generating process.

There are two obvious approaches for specifying the bandwidth for temperature. This can be any fixed width in degrees Celsius, or any fixed number of months as per the standard fitting procedure. Because of the potential subjectivity of fixing a user specified bandwidth, the latter is preferred. A fixed number of months will result in different bandwidths measured in degrees Celsius, because of the variability in mean monthly temperature throughout the year.

Selecting a fixed number of months is analogous to using the K-nearest neighbour (KNN) algorithm to classify the data in only one dimension with K equal to the selected number of months. Observations (y) are selected according to their Euclidean distance (d) from a chosen value (x) using Equation 1:

$$d(x, y) = \sqrt{(x_1 - y_1)^2} \equiv |x_1 - y_1| \tag{1}$$

where $x_1$ and $y_1$ are the target and observed values for the single predictor. The training data for model fitting at target value (x) is therefore based on the K nearest observations, or the top K months taken from the rank of all calculated distances.

Parameter estimation is performed using a Generalised Method of Moments (GMM) with a weighted least squares objective function: $S(\boldsymbol{\theta} \mid \boldsymbol{t}) = \sum_{i=1}^{k} \omega_i [t_i - \tau_i(\boldsymbol{\theta})]^2$, where $\boldsymbol{\theta} = (\theta_1, \ldots, \theta_p)^\mathsf{T}$ is the vector of p model parameters, $\boldsymbol{t} = (t_1, \ldots, t_k)^\mathsf{T}$ is the vector of k observed summary statistics, $\boldsymbol{\tau(\theta)} = (\tau_1(\boldsymbol{\theta}), \ldots, \tau_k(\boldsymbol{\theta}))^\mathsf{T}$ is the vector of k expected summary statistics, and $\omega_i$ is a weighting applied to the i-th summary statistic. The GMM minimisation routine employed in this research is performed using an updated version of the MOMFIT software developed by Chandler et al. (2010). This software uses asymptotic theory to provide parameter estimators which are multivariate normally distributed (MVN). This captures the known dependence between BLRP model parameters, and enables parameter uncertainty to be propagated forward into the estimation of rainfall summary statistics and extremes. The mean of the MVN distribution is the optimal parameter set, and the variance-covariance matrix is estimated from the least squares objective function $S(\boldsymbol{\theta} \mid \boldsymbol{t})$ (Chandler et al., 2010).

For consistency with the analysis and results presented in Cross et al. (2018), the downscaling approach is tested using the same three variants of the BLRP rainfall models: the original model (BL0) by Rodriguez-Iturbe et al. (1987), the modified model (BL1) by Rodriguez-Iturbe et al. (1988) in which the rain cell duration parameter $\eta$ is randomized, and the modified model with rain cell intensity $\mu_x$ also randomised (BL1M) by Kaczmarska et al. (2014). Table A.4 in Appendix A compares the parameters of the three BLRP model variants and provides the units for each parameter. Following the standard fitting procedure for seasonally varying parameters, rainfall summary statistics are calculated for each month of the historical record. However, to fit the BLRP models using the GMM, it is necessary to select rainfall summary statistics coincident with selected covariate target values. This is described in the following section.

### *3.2. Covariate target range*

KNN sampling can be applied to any covariate target value within or outside the observed covariate range. However, for target values close to the extremes of the observed covariate range, samples of historical months become increasingly unrepresentative of the target value because of the increasing scarcity of unique historical records. Because the downscaling methodology involves regression on the parameter estimators, it is necessary to ensure that the selection of fitting months is representative of the covariate target values. This gives rise to a covariate target range which is inevitably narrower than the observed range. As K increases, the covariate target range used for model fitting reduces. This is shown graphically in Fig.2 for Bochum using the historical temperature projections from the IPSL-CM5A-MR climate model (see Sect.4.2 for a description of the climate model data) with K fixed at 52, 104 and 156 months (see Sect.4.1 for a description of the rain gauge data).

At Bochum, the mean monthly near surface air temperature ranges from -6.8 to 22.5 °C. For covariate target values incremented at 1 °C, an initial target range would span -6 to 22 °C as shown by the series of box and whisker plots in Fig.2. It can be seen in Fig.2 that most selections closely follow the 1:1 line with both mean and median temperatures within the selection very close to the target value. However, this is not true at the extremes of the covariate range with several target values comprising identical selections with mean temperatures which deviate significantly from the target value (grey box and whisker plots). Identical selections would result in identical BLRP parameter estimators. The covariate target range is therefore refined to remove these identical selections, and those where the mean of the selection (magenta line) deviates by more than 1 °C from the target value. For $K = 52$, these include -6, -5, -4, -3, -2, -1, 21, and 22 °C (see Fig.2). Therefore, for $K = 52$ months, the covariate target range is 0 to 20 °C shown by the series of blue box and whisker plots in Fig.2. Assuming that the selection bandwidth is defined by the total extent of the whiskers, the bandwidths for $K = 52$ range between approximately 1 and 5 °C.

### *3.3. Model parameter regression*

We hypothesize that mechanistic-stochastic rainfall model parameter estimators may be approximated by regression without significant detriment to rainfall simulation and the estimation of extremes. Therefore, upon the calibration of model parameters for the full range of target values (Sect. 3.2), the relationship between parameter set estimators and temperature is approximated using multivariate linear regression. In this framework, we have multiple dependent (response) variables, the set of BLRP parameter estimators, and

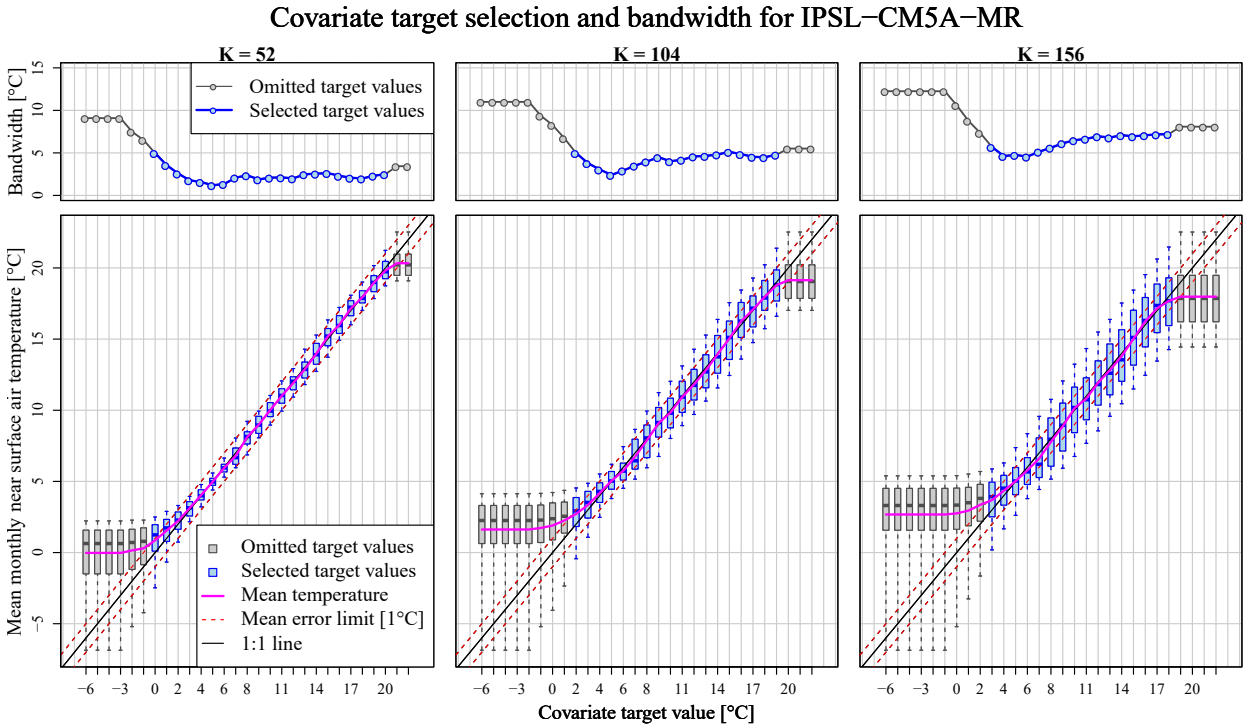


Figure 2: Example covariate target selection for Bochum using CMIP5 climate model IPSL-CM5AMR historical model run (r1i1p1 ensemble). Selection is based on K fixed at 52, 104, and 156 resulting in variable bandwidths shown in the top panel.

one independent (predictor) variable, our chosen covariate the mean monthly near surface air temperature. The multivariate regression framework enables us to preserve the dependence between model parameters and is performed on the natural logarithm of the parameter estimators for consistency with BLRP fitting methodology. Using the regression model, we can estimate parameters within and beyond the range of present day monthly mean temperatures enabling estimation of rainfall extremes under hypothesised warmer climates.

For $n$ observations, $m$ response variables and $p$ predictor variables, the multivariate regression model takes the form given in Equation 2:

$$\mathbf{Y_{n\times m}} = \mathbf{X_{n\times(p+1)}}\boldsymbol{\beta}_{\mathbf{(p+1)\times m}} + \boldsymbol{\epsilon}_{\mathbf{n\times m}} \tag{2}$$

where $\mathbf{Y}$ is the $n \times m$ matrix of response variables, $\mathbf{X}$ is the $n \times (p+1)$ design matrix for predictor variables, $\boldsymbol{\beta}$ is the $(p+1) \times m$ matrix of regression coefficients, and $\boldsymbol{\epsilon}$ is the $n \times m$ error matrix. For our regression model, $n$ is the number of covariate target values, $m$ is the number of BLRP model parameters, and $p = 1$ for the single predictor covariate, the mean monthly near surface air temperature. The matrix expansion of Equation 2 is given in Equation 3:

$$\begin{pmatrix} y_{1,1} & \cdots & y_{1,m} \\ \vdots & \ddots & \vdots \\ y_{n,1} & \cdots & y_{n,m} \end{pmatrix} = \begin{pmatrix} 1 & x_{1,p_1} \\ \vdots & \vdots \\ 1 & x_{n,p_1} \end{pmatrix} \begin{pmatrix} b_{0,1} & \cdots & b_{0,m} \\ b_{p_1,1} & \cdots & b_{p_1,m} \end{pmatrix} + \begin{pmatrix} e_{1,1} & \cdots & e_{1,m} \\ \vdots & \ddots & \vdots \\ e_{n,1} & \cdots & e_{n,m} \end{pmatrix} \tag{3}$$

where the subscript $p_1$ refers to the single predictor variable, here the mean monthly near surface air temperature.

Upon fitting the regression model, we obtain the matrix of regression coefficients and their error matrix which describes the regression uncertainty. With these we can approximate the set of BLRP parameter estimators for new observations within and beyond the covariate target range used to fit the regression. For

the simulation of rainfall extremes using the BLRP models, it is desirable to specify the multivariate normal distribution of parameter estimators so that realistic simulation bands may be produced incorporating parameter uncertainty [1]. This requires the mean of the distribution which is the optimal parameter set, and its corresponding variance-covariance matrix which describes the rainfall model uncertainty. In the downscaling approach, the mean of the distribution is replaced by the regression estimates at the target values. However, the rainfall model uncertainty needs to be updated to incorporate the regression uncertainty to obtain the combined temperature conditioned model uncertainty.

The regression uncertainty comprises two sources of error which arise from predicting the response variables for new observations from the regression model. The first describes the positions of the regression lines at the prediction value, and the second the variance around this. Assuming $\mathbf{Y_i}$ is the predicted response vector for the *ith* observation $X_i$, the variance of the expectation of response variables $\mathbf{E}\big[\mathbf{Y_i}\big]$ - which describes the position of the regression lines - is $\mathbf{var}(\boldsymbol{\beta}^{\mathsf{T}}\mathbf{X_i} - \hat{\boldsymbol{\beta}}^{\mathsf{T}}\mathbf{X_i})$ where $\hat{\boldsymbol{\beta}} = (\mathbf{X_i}^{\mathsf{T}}\mathbf{X_i})^{-\mathbf{1}}\mathbf{X_i}^{\mathsf{T}}\mathbf{Y_i}$ is the least squares estimate of $\boldsymbol{\beta}$. The variance of the response variables around the regression lines is $\mathbf{var}(\mathbf{Y_i} - \hat{\boldsymbol{\beta}}^{\mathsf{T}}\mathbf{X_i})$. Setting $\boldsymbol{\Sigma} = \mathbf{var}(\boldsymbol{\epsilon})$, the prediction variance is $\boldsymbol{\Sigma}\big[\mathbf{1} + \mathbf{H}\big]$ where $\mathbf{H} = \mathbf{X}(\mathbf{X}^{\mathsf{T}}\mathbf{X})^{-\mathbf{1}}\mathbf{X}^{\mathsf{T}}$. Predicted response variables are assumed to be multivariate normally distributed, hence we have the distribution of response variables given in Equation 4.

$$\mathbf{Y} - \hat{\boldsymbol{\beta}}^{\mathsf{T}}\mathbf{X} \sim \mathbf{MVN}\Big[\mathbf{X}\hat{\boldsymbol{\beta}}, \boldsymbol{\Sigma}\big[\mathbf{1} + \mathbf{H}\big]\Big] \tag{4}$$

The regression error variance $\boldsymbol{\Sigma}$ is unknown, therefore the unbiased estimate of the error variance for covariate $X_i$ is $\widehat{\boldsymbol{\Sigma}_\mathbf{i}} = \mathbf{SSCP}_{\boldsymbol{\epsilon}\mathbf{i}}/(\mathbf{n} - \mathbf{p} - \mathbf{1})$ where $\mathbf{SSCP}_{\boldsymbol{\epsilon}\mathbf{i}} = \widehat{\boldsymbol{\epsilon}_\mathbf{i}}^{\mathsf{T}}\widehat{\boldsymbol{\epsilon}_\mathbf{i}}$ is the sum of squares and cross products of the residuals. Therefore, the estimated prediction variance of response variables $\mathbf{Y_i}$ - the regression uncertainty - is $\mathbf{var}(\mathbf{Y_i} - \hat{\boldsymbol{\beta}}^{\mathsf{T}}\mathbf{X_i}) = \hat{\boldsymbol{\Sigma}}_\mathbf{i}\big[\mathbf{1} + \mathbf{H}\big]$. This is added to the variance of the BLRP parameter estimators - the rainfall model uncertainty - to obtain the updated variance for the BLRP parameters, the temperature conditioned model uncertainty. For predicted BLRP parameter estimators beyond the range of observations, either the variance for the nearest BLRP parameter estimator can be used or the mean of the BLRP parameter variances. Therefore, the multivariate normal distribution of predicted BLRP parameter estimators from the regression model, $\hat{\mathbf{Y}}_\mathbf{BLRP}$, is given in Equation 5 where $\bar{\boldsymbol{\Sigma}}_\mathbf{BL}$ is the mean rainfall model uncertainty.

$$\hat{\mathbf{Y}}_\mathbf{BLRP} \sim \mathbf{MVN}\Big[\mathbf{X}\hat{\boldsymbol{\beta}}, \hat{\boldsymbol{\Sigma}}\big[\mathbf{1} + \mathbf{H}\big] + \bar{\boldsymbol{\Sigma}}_\mathbf{BL}\Big] \tag{5}$$

### *3.4. Simulation and weighting of ensemble extremes*

When the conditioning covariate is changed to mean monthly air temperature, the number of parameter sets used to capture the annual variation in rainfall depends on the increments over which the BLRP model is fitted, and the covariate target range. The estimated BLRP parameters then become the data used to fit the regression model, which has only 10 regression parameters, the intercept ($b_0$) and slope ($b_p$) of the separate BLRP parameter regressions (example regression parameters for the NCEP conditioned BLRP models are provided in Table C.6 in Appendix C). Despite this, rainfall simulation is performed in the standard way with 12 parameter sets (or BLRP models), one for each calendar month of the year. In the downscaling framework, the monthly BLRP parameter sets are estimated from the regression model.

Rainfall simulation follows the same procedure as that set out in Cross et al. (2018) by randomly sampling $N$ times from the distribution of BLRP parameter estimators to generate N realisations of simulated rainfall above the predefined censor. By sampling from the updated multivariate normal distribution of BLRP parameter estimators given in Equation 5, the spread of realisations generates simulations bands which capture the different sources of error in the model. These include the rainfall model uncertainty, the regression uncertainty, and the sampling uncertainty which arises in simulation.

[1] The BLRP parameter estimators are asymptotically normally distributed.

For the estimation of rainfall extremes, mean monthly near surface air temperatures are selected from climate model outputs using an ensemble of CMIP5 models. The rainfall models are initially calibrated using the historical climate model run before applying the regression model to BLRP parameter estimators. Then, present and future climate extremes are estimated using mean monthly air temperature sampled from the historical and future climate model simulations respectively. For the estimation of future extremes, temperature projections are obtained corresponding to a chosen representative concentration pathway (RCP, see Moss et al. (2010) and Vuuren et al. (2011)) and time slice. The latter may represent any future period typically 30 years in duration up to 2100, the temporal extent of most climate model runs. Hence, estimation for a high concentration pathway in the far future would use the climate model projection for RCP8.5 spanning 2070-2100. From this 30-year time-slice, the mean monthly air temperature for each calendar month is calculated and used as a new observation in the regression model to generate the distribution of BLRP parameter estimators for simulation.

The benefit of using an ensemble of climate model runs in the estimation of rainfall extremes is to reduce the bias of individual climate models. However, it is recognised that some climate conditioned rainfall models will perform better at estimating rainfall extremes than others. Therefore, a simple weighting is applied to each model according to its ability to reproduce 5-minute rainfall extremes estimated from reanalysis conditioned rainfall models for the present climate. Extremes are estimated for a range of return periods using simulated annual maxima.

A weighted root mean square error (RMSE) score is calculated for each climate conditioned model which applies greater weight to the ability of the models to reproduce higher return period extremes. This approach was chosen to ensure that all extremes were used in the weighting, while placing greater importance on the larger extremes. While it is recognised that larger extremes have larger variance, these extremes are more likely to be representative of convective summer storms than the more frequent ones. The weighted RMSE gives relative scores for each climate conditioned model enabling them to be ranked according to their extreme value performance. This ranking is used to weight the quantiles of the extreme value estimates across all realisations thereby generating weighted median and 95% simulation bands.

## 4. Data

### *4.1. Rain gauge data*

The downscaling of fine scale rainfall extremes with censoring for hypothetical warming climates using the methodology set out in Section 3 is performed for the two rainfall datasets used to present the censored approach for the estimation of fine-scale extremes in Cross et al. (2018); Bochum in Germany and Atherstone in the UK. Both datasets were chosen for their quality and length (69 and 48 years), because the methods of recording is different (Hellmann floating pen and tipping bucket gauges respectively), and because of their different locations. The Bochum data are aggregated to the 5-minute temporal resolution, while tip-time data can be aggregated to any scale.

Guided by the results presented in Cross et al. (2018), the downscaling approach is performed for 5-minute accumulations using a constant censor of 0.5 mm at both sites. For Bochum, downscaling is based on a subset of the rainfall record from 1948 to 1999 to coincide with the data range of the NCEP reanalysis data (Sect.4.3) which is used for climate model weighting and BLRP model validation (Sect.5). The Atherstone dataset commences in 1967 after the start of the NCEP reanalysis data on January 1st, 1948, and extends to 2015.

### *4.2. Climate model data*

In this study, both present and future climate extremes are estimated using an ensemble of long-term historical and future RCP climate simulations from phase 5 of the Climate Model Intercomparison Project (CMIP5, Taylor et al., 2012). The CMIP5 experiments provide climate projections for a range of common scenarios in a multi model context. They are differentiated by their starting point in the pre-industrial control period (realisation), their initialisation method and physics (physical constraints or parameterisation) and are identified by the rip-nomenclature: (r)ealisation-(i)nitialisation-(p)hysics. To test the downscaling

methodology, only long-term simulations relating to ensemble number r1i1p1 were used with two climate forcing scenarios, RCP4.5 and 8.5, chosen to be indicative of moderate to severe climate change. A total of 29 models within the suite of CMIP5 climate models were identified with the historical and two future scenarios available. These are listed in Table B.5 in Appendix B. The output variable from these climate models used for analysis is the mean monthly near surface air temperature with the common abbreviation, *"tas"*. Historical and future time-series were sampled for the closest climate model grid squares to the gauge latitude and longitude locations; (51.49, 7.22) and (52.58, 358.47) for Bochum and Atherstone respectively.

### *4.3. Climate reanalysis data*

The reanalysis data used for climate model weighting and BLRP model validation is the NCEP/NCAR (National Centers for Environmental Prediction) Reanalysis 1 model output from the National Oceanic and Atmospheric Administration (NOAA) Earth Systems Research Laboratory (Kalnay et al., 1996). Outputs for the mean monthly near surface air temperature are used for grid squares closest to the gauge latitude and longitude locations, (51.49, 7.22) and (52.58, 358.47) for Bochum and Atherstone respectively, which are available from January 1st, 1948 .

## 5. Calibration and validation

### *5.1. Model fitting and simulation*

The estimation of fine-scale rainfall extremes in a changing climate with censoring is first performed for the present climate. Both censored and uncensored extremes (extremes obtained with and without censoring applied) are estimated to confirm that similar improvement in estimation to that observed in Cross et al. (2018) is achieved when the conditioning variable is changed to mean monthly near surface air temperature. Annual maxima are sampled directly from simulations and the estimation of extremes is based on the weighted 50th quantile (wQ50) with 95% simulation bands given by weighted 2.5th and 97.5th quantiles, wQ2.5 and wQ97.5 respectively. The calibration methodology and conditioning information is set out in the remainder of this section. Section 5.2 presents the results of the model calibration and regression, and Sect.5.3 the results of the validation.

The choice of fitting statistics at each gauge location is summarised in Table 1 with timescales given in brackets. Because the Gamma shape parameter $\alpha$ in the two randomised models, BL1 and BL1M, is insensitive and can take a wide range of values without significant impact on the estimation of extremes Cross et al. (2018), it is held fixed at 100 and 5 respectively. The ratio of the standard deviation to mean of the cell depth $r = \sigma_x/\mu_x$ is fixed at 1 for all three models, thereby specifying the exponential distribution for the mean cell intensity. By holding these parameters fixed, optimisation is only required for 5 parameters in each model: BL0 $(\lambda, \beta, \mu_x, \eta, \gamma)$, BL1 $(\lambda, \kappa, \mu_x, \nu, \phi)$, and BL1M $(\lambda, \kappa, \iota, \nu, \phi)$.

Table 1: Summary of fitting statistics for BLRP rainfall model calibration. The temporal resolution of the fitting statistics used is provided in brackets the table with units of hours (h).

| | **Un-censored (h)** | **Censored (h)** |
|---|---|---|
| Bochum | Mean[1] (1), coefficient of variation (0.083,6,24), skewness (0.083,6,24), lag 1 autocorrelation (0.083,6,24) | Mean (1), coefficient of variation (0.083 6,24), lag 1 autocorrelation (0.083,6,24) |
| Atherstone | Mean (1), coefficient of variation (0.083,1,6,12,24), skewness (083,1,6,12,24), lag 1 autocorrelation (0.083,1,6,12,24) | Mean (1), coefficient of variation (0.083,1,6,24), lag 1 autocorrelation (0.083,1,6,24) |

1. The mean, coefficient of variation, skewness and autocorrelation are all calculated on the aggregated rainfall intensities including dry periods (0 mm rainfall) for the un-censored and censored rainfall time-series respectively.

For each of the climate conditioned BLRP rainfall models, 40 time-series realizations are simulated with duration equivalent to the duration of the observed record, 47 years at Atherstone and 52 years at Bochum.

This number of realisations is large enough to give a robust estimation of the median extreme rainfall required for individual model weighting. But because the total ensemble of climate conditioned models is large with 29 members the resulting number of realisations for estimation of the wQ50 is very large, 1160 realisations.

Each realization is generated using a different parameter set sampled from the multivariate normal distribution of model parameter estimators given in Equation 5 hereafter referred to as MVN realizations . The fitting window is based on K equal to the duration of the rainfall records in years, 47 and 52 months for Atherstone and Bochum respectively. By analogy with the standard fitting methodology this is equivalent to using one calendar month, albeit months may be selected from anywhere in the rainfall record according to their historical mean monthly air temperature.

Initial model fitting using this approach resulted in some parameter sets being poorly identified. In these cases, K is increased by including additional months from the selections for adjacent target values. This procedure is repeated until the upper limit on parameter uncertainty for all model parameters is reduced to below an arbitrary threshold of 250 (units vary for each paramter, see Table A.4 in Appendix A), or for a maximum of 5 iterations. By including additional months from adjacent selections in this way the fitting window is effectively widened locally with K for subsequent target value parameterisations returning to the original selections.

### *5.2. Bartlett-Lewis parameter estimators*

Figure 3 shows the full range of censored BLRP model parameter estimators conditioned on near surface air temperature using outputs for the historical periods for each of the 29 CMIP5 climate models and the NCEP reanalysis data. The plots reveal a clear dependence between temperature and several of the BLRP model parameters at both locations including: increasing relations in the storm arrival rate ($\lambda$), mean cell depth ($\mu_x$) or ratio of mean cell depth to cell duration ($\iota$), and decreasing relations in the cell duration parameter ($\eta$) or the ratio of the Gamma shape and scale parameters ($\alpha/\nu$) for the randomised models. The remaining parameters – cell arrival rate ($\beta$), storm duration ($\gamma$), and the ratios of cell arrival rate and storm duration to cell duration ($\kappa$ and $\phi$ respectively) - show less obvious relations. Broadly the relations appear to follow the same pattern at both sites and the spread of parameter estimators across all 29 CMIP5 climate models, and the NCEP reanalysis, is small, indicating high consistency in the fitting. It is also noted that the NCEP conditioned parameter estimators sit inside the range of the 29 CMIP5 climate model conditioned estimators as would be expected for reanalysis data.

By means of an example, the fitted regression relationships with associated uncertainties for the NCEP conditioned rainfall models are shown in Figure 4. The plots show the rainfall model uncertainty (magenta polygons, *NCEP cond. 95 % BL estimator CIs*), regression uncertainty (blue polygons, *BLRP 95 % regression PIs*), and the combined climate conditioned BLRP model uncertainty (blue dashed lines, *BLRP 95 % regression uncertainty*). As noted in Sect.3.3, the regression uncertainty comprises two additive error sources which when combined comprise the prediction intervals (PIs) for the regression model.

Multivariate analysis of variance (MANOVA) is used to simultaneously test the response of the BLRP parameter estimators to the NCEP mean monthly near surface air temperatures. The primary test statistics, Pillai's trace, the approximate F-statistic which determines the significance level of the regression, and the p-value associated with the F-statistic are provided in Table 2. For all three models at both locations the p-value is very small indicating that the F-statistic is highly significant and consequently the null hypothesis that temperature has no effect on the mean BLPR parameter estimators is rejected. The high Pillai trace values demonstrate that temperature is highly informative for each of the fitted regressions.

While the p-values in Table 2 indicate that we can reject the null hypothesis of no relationship for the multivariate regressions, testing each variable individually with a univariate analysis of variance (ANOVA) (Appendix C, Table C.6) shows that for some BLRP parameter estimators such as the cell arrival rate ($\beta$) and storm duration ($\gamma$) in the BL0 model, there are little or no differences in their means at the 5 % significance level (p-values $> 0.05$). Correspondingly we see that the coefficient of determination ($R^2$) for those parameters is low indicating that only a small percentage of the variance in those parameters is explained by their individual regressions. However, their inclusion in the multivariate regression is important

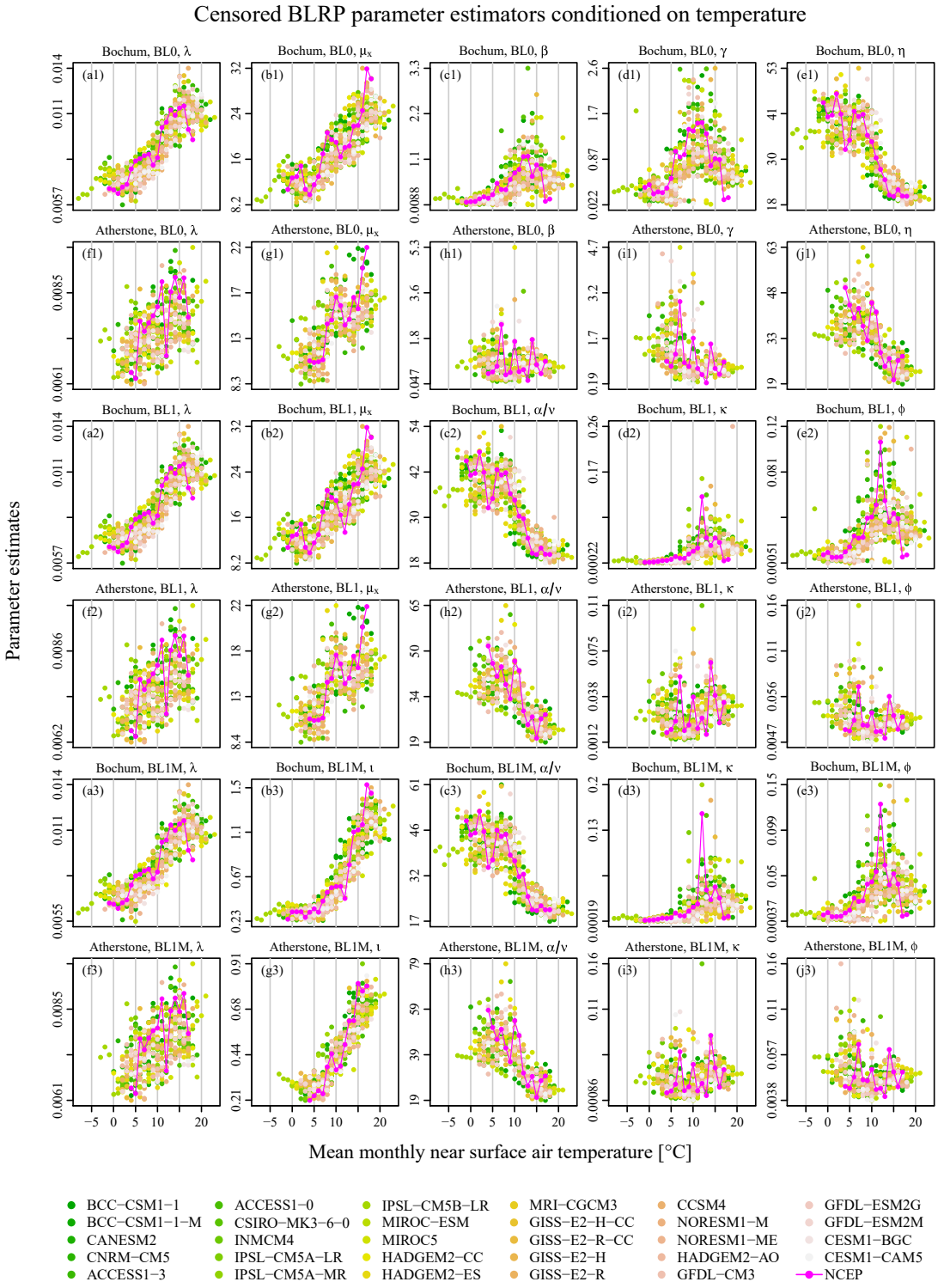


Figure 3: Scatter plots showing the response of censored BLRP parameter estimators for Atherstone and Bochum conditioned on mean monthly near surface air temperature for each of the 29 CMIP5 historical model runs, and NCEP reanalysis data.

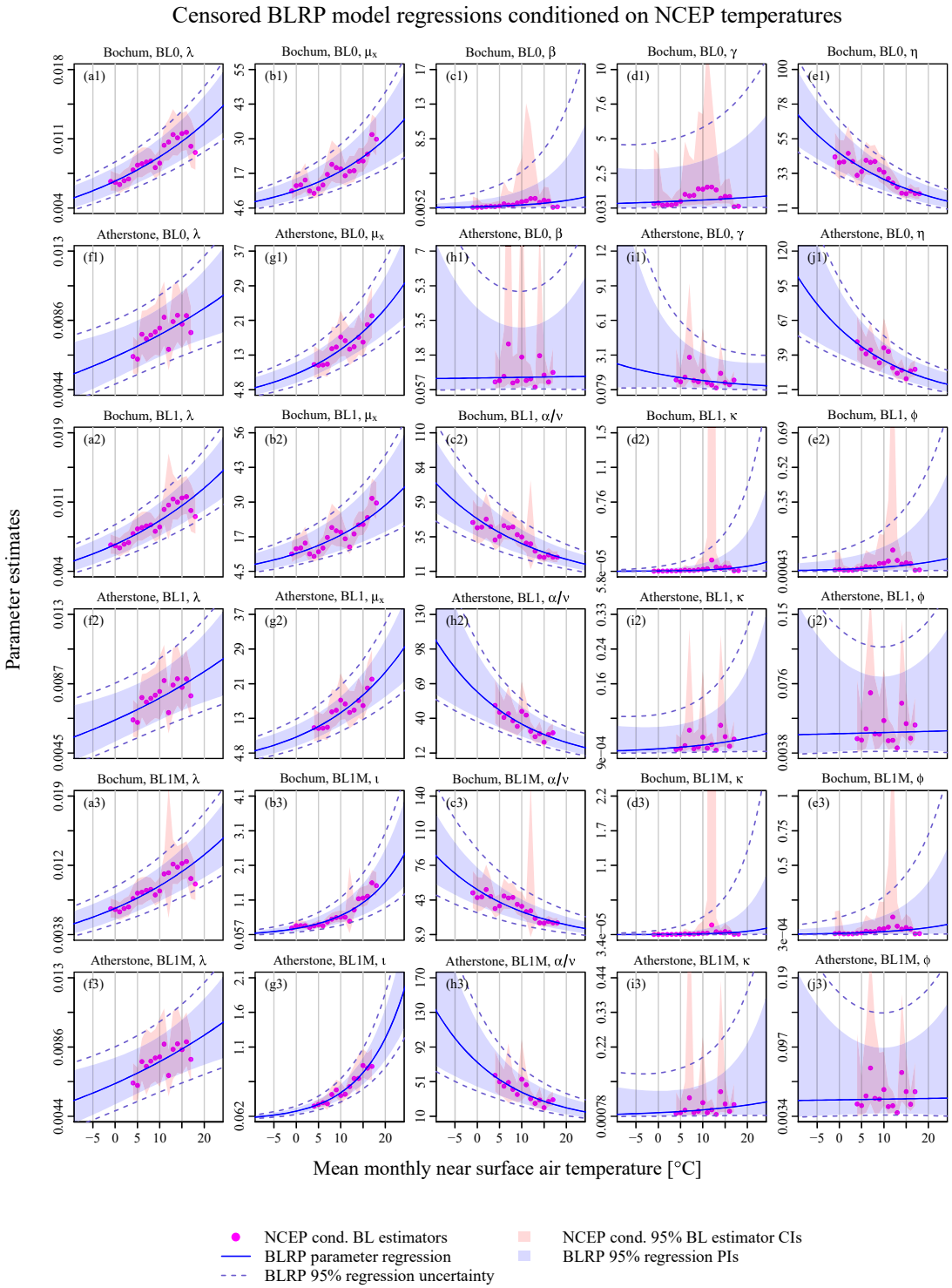


Figure 4: Censored BLRP model parameter regressions for Atherstone and Bochum conditioned on mean monthly near surface air temperatures for the NCEP reanalysis data. Plots show the location of the parameter regressions, their associated prediction interval (PIs) and updated BLRP 95% regression uncertainty.

Table 2: Multivariate analysis of variance (MANOVA) summary results for the NCEP conditioned Bartlett-Lewis parameter regression models.

| Model | Location | Pillai | Approx. F | $P(>F)$ |
|---|---|---|---|---|
| BL0 | Bochum | 0.9765 | 116.51 | $6.77 \times 10^{-11}$ |
| | Atherstone | 0.9768 | 67.27 | $2.56 \times 10^{-6}$ |
| BL1 | Bochum | 0.9753 | 110.57 | $9.66 \times 10^{-11}$ |
| | Atherstone | 0.9768 | 67.24 | $2.56 \times 10^{-6}$ |
| BL1M | Bochum | 0.9729 | 100.48 | $1.85 \times 10^{-10}$ |
| | Atherstone | 0.9769 | 67.73 | $2.49 \times 10^{-6}$ |

for the estimation of the variance-covariance of model parameters. The regression parameter estimators, $b_0$ and $b_p$ in Equation 2, are also shown in Appendix C, Table C.6. Because the regressions are performed on the natural logarithm of the rainfall model parameters, the units of $b_0$ are the natural logarithm of the rainfall model parameter units, and the units of $b_p$ are same but per Kelvin.

The plotted regressions are shown extending beyond the range of observations used for fitting to indicate the nature of the regressions when extrapolating. Where the parameter response is broadly flat – cell arrival rate ($\beta$), storm duration ($\gamma$), and the ratios of cell arrival rate and storm duration to cell duration ($\kappa$ and $\phi$ respectively) – the regression uncertainties grow much more quickly. This is likely to result from one or several BLRP parameter estimators lying further away from the best fit regression line thereby increasing the error variance of the regression model. Greater error variance is likely to arise in parameters which are relatively (to the other model parameters) less sensitive to the training data. This may also be indicative of multiple fitting regions in the BLRP parameter space, resulting in larger deviations in the fitted parameters between some covariate target values.

Because all fitted BLRP parameter estimators are well identified, they are assumed to be robust estimators for inclusion in the regression model. However, it is recognised that the rapid growth in regression uncertainty may be an issue when sampling from the MVN distribution of parameter estimators in simulation if the estimation of extremes is sensitive to large deviations in these parameters from their mean.

The regression uncertainty (blue polygons in Fig.4), show the 95% PIs for the multivariate regression. A visual inspection of the regression plots shows that in most instances the PIs bracket most of the fitted BLRP parameter estimators. Exceptions include Bochum BL0 ($\beta$), BL1 ($\lambda, \kappa$), and BL1M ($\lambda, \iota, \kappa$) where only a few parameters fall just outside the PIs. None of the estimators for Atherstone appear to fall outside the 95% PIs. This level of accuracy can reasonably be expected and indicates that the regression fitting is successful. The updated climate conditioned BLRP uncertainty (blue dashed lines, *BLRP 95 % regression uncertainty*, in Fig.4) are consistently wider than the regression uncertainty and do bracket all BLRP parameter estimators, and much more of the rainfall model uncertainty. It is important to capture as much of the rainfall model uncertainty as possible to ensure that range over which BLRP parameter estimators are randomly sampled in simulation is characteristic of the original rainfall model fitting.

### *5.3. Replication of summary statistics*

It is important to verify that the sampling of regressed parameters from the multivariate normal distribution given in Equation 5 provides BLRP parameter sets which satisfactorily reproduce the statistical profile of the data to which they are fitted. Given that it is neither possible to validate larger extremes in the current climate, nor extremes in any hypothesised changed climate, validation of the process upon which these extremes are generated is essential for the extreme value estimates to be credible.

Validation is performed in the standard way for mechanistic stochastic rainfall models. First, we verify that the parameter estimators can reproduce the summary statistics used to derive them. While it seems intuitive that they would, this is not always true if the parameters are poorly identified or the objective function value is significantly different from zero. Next, we check how well the BLRP parameter estimators

reproduce other summary statistics not used in the fitting. Because of the two-stage fitting process used in this study, validation statistics are presented for the BLRP parameter estimators used to fit the regression model, and BLRP parameter estimators derived from the regression model at the target covariate values. While there are many models in the CMIP5 ensemble, validation statistics are only calculated for the NCEP conditioned BLRP model because the bias of reanalysis outputs is marginal, and the NCEP conditioned extreme value estimates are used to weight the performance of the 29 CMIP5 conditioned BLRP models.

Figure 5 shows the variation in censored 5-minute rainfall summary statistics used to fit the BLRP models – mean, coefficient of variation, and lag-1 autocorrelation (see Table 1) - with mean monthly near surface air temperature. For validation of the fitting statistics, the mean rainfall is re-scaled from 1 hour to 5 minutes. The top 6 panels show the variation in summary statistics for fitted model parameters at both locations, and the bottom 6 panels the equivalent statistics for estimated parameters using the regression model in Equation 5. Figure 6 shows the ability of the models to reproduce a selection of validation statistics not used in the fitting: the variance, lag-1 autocovariance, and proportion of wet periods. Skewness has been left out of this selection because, as highlighted in Cross et al. (2018), the BLRP models are not expected to reproduce the skewness well for censored data.

At Bochum, the target covariate values for the NCEP reanalysis data range from -1 to 18 °C, and at Atherstone from 4 to 17 °C, in each case at 1 °C increments. Summary statistics are estimated under each BLRP model variant using 100 parameter sets randomly sampled from the MVN distribution of parameter estimators and used to generate simulation bands from the 2.5th and 97.5th quantiles. The observed summary statistics are calculated from the selection of rainfall months corresponding to the separate target covariate values. Summary statistics relating to the mean of the distribution are also calculated using the optimal parameter sets.

All three models perform equally well in replicating both the fitting and validation statistics with little variation in the statistics estimated by each of the models for all target covariate values. The only exception to this is the performance of the BL1 and BL1M models at Bochum for the target value of 12 °C where the width of the simulation bands on the estimated summary statistics diverges. This divergence occurs because the parameter set for 12 °C is less well identified than those at the other target values (see Fig.5, Bochum BL1 and BL1M $\kappa$ and $\phi$). The 95 % simulation bands for the estimated fitting statistics comfortably bracket the observed for all target covariate values despite their narrow range (except for 12 °C in Bochum, see Fig.5). Conversely, the simulation bands for the validation statistics do not always bracket the observed at the target covariate values (Fig.6). There is very good agreement between the estimated and observed validation summary statistics at Bochum with the proportion of wet periods only falling outside the simulation bands once at target value 4 °C.

The BLRP regression model parameters perform very well in reproducing the fitting and validation statistics. The response of the estimated summary statistics under the regressed parameter estimators is much smoother than with the fitted parameters, which is expected. However, the response clearly follows the apparent underlying dependence in statistics with temperature, indicated by the observations. This is a very pleasing result as the regression is performed on the parameter estimators themselves, and not the observations. The simulation bands appear to be slightly wider than those for the fitted model parameters which is also expected because of the additional regression error, and they comfortably bracket all observed fitting statistics and most observed validation statistics. The only exceptions here occur in the estimation of validation statistics at Atherstone where the observed lag-1 auto-covariance falls outside the simulation bands at 9, 10, and 14 °C, and the proportion of wet periods fall outside the simulation bands between 4 and 7 °C. These results support the hypothesis that mechanistic rainfall model parameters may be approximated by regression without significant detriment to rainfall simulation.

A notable observation about the rainfall statistics shown in Figs.5 and 6 is their interesting temperature dependence. The coefficient of variation and lag-1 autocorrelation show approximate linear relations with increasing temperatures (falling and rising respectively), while all other statistics show non-linear rising relations which, for the mean, variance, and lag-1 auto-covariance, appear nearly flat for colder temperatures, especially at Bochum where the temperatures drop to -1 °C. Because these dependencies are characteristic of rainfall over a low censor, they demonstrate that intense rainfall is strongly influenced by the near surface air temperature. This is important for capturing rainfall extremes arising from different rainfall events and

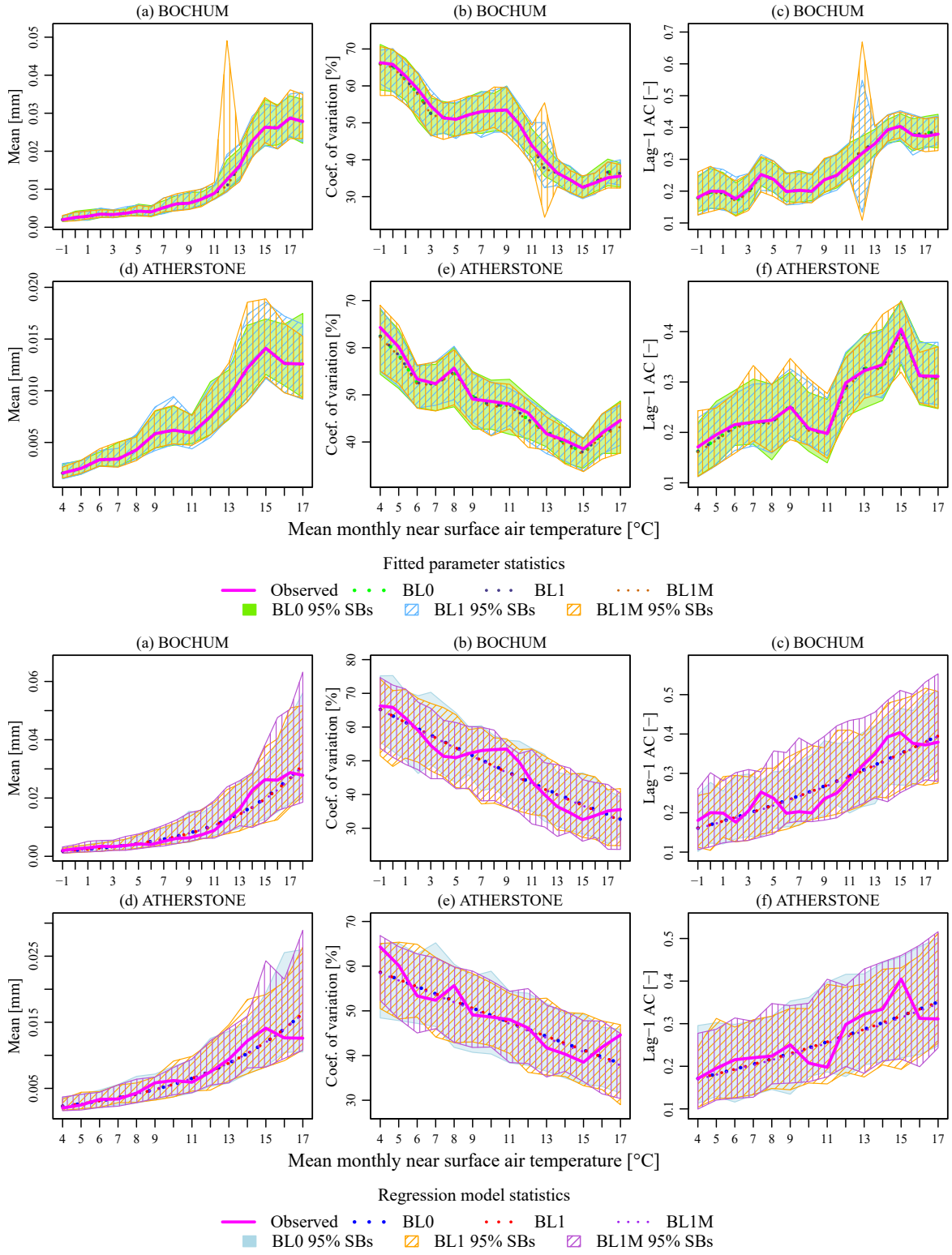


Figure 5: Variation in censored 5-minute rainfall calibration statistics - mean, coefficient of variation and lag-1 autocorrelation - with mean monthly near surface air temperature for fitted and regressed BLRP parameter estimators.

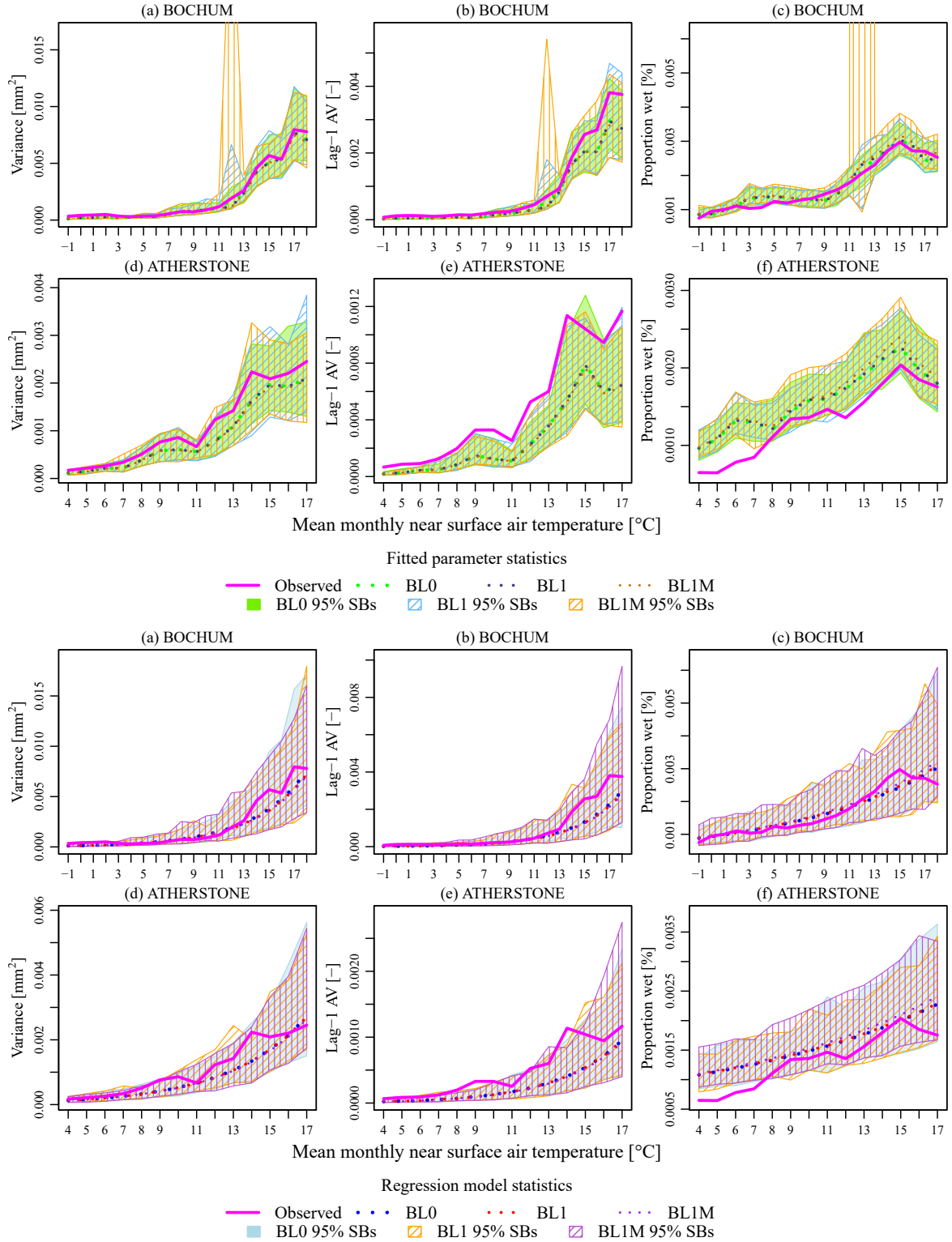


Figure 6: Variation in censored 5-minute rainfall validation statistics - variance, lag-1 autocovariance and proportion of wet periods - with mean monthly near surface air temperature for fitted and regressed BLRP parameter estimators.

potentially offers an improvement over fitting to calendar month where both stratiform and convective events may be lumped together in any of the summer months. It is therefore particularly pleasing that the nature and variation of these dependencies is well captured by both the rainfall model, and temperature dependent regression model parameters.

For the purpose of estimating rainfall extremes with censoring, these statistics demonstrate that the models are well parameterised and that the process of rainfall generation on which the estimation of extremes depends is robust. The plots in both figures also show that important central moments of the rainfall time-series are strongly correlated with temperature, supporting the selection of near surface air temperature as an appropriate conditioning covariate.

## 6. Extreme rainfall estimation

Figures 7 and 8 show the estimation of 5-minute rainfall extremes at Bochum and Atherstone respectively for the complete ensemble of 29 CMIP5 climate model conditioned BLRP rainfall models. Estimation is shown for all three BLRP models, and three climate scenarios, historical (hist), medium carbon forcing (rcp45) and severe carbon forcing (rcp85). The plots also include un-censored estimation for the present climate to demonstrate the benefit of censoring for extreme rainfall estimation. Tables D.7 and D.8 in Appendix D provide the 10 and 100-year return period weighted extreme rainfall estimates in mm for Bochum and Atherstone respectively corresponding to the plots given in Figures 7 and 8, as well as the width of the 95 % simulation bands (SBs) at those return periods [2].

The first and most important observation from the plots in Figs.7 and 8 is that the estimation of rainfall extremes with temperature dependent censored rainfall modelling for the historical period is very good. Consistent with the estimation of short duration extremes by mechanistic stochastic rainfall models, fitting to the whole (un-censored) rainfall hyetograph results in their under-estimation (grey lines and simulation bands).

The improvement in extreme rainfall estimation with censoring is very similar to that in Cross et al. (2018), with the BL1M model once again performing slightly better than the other two, and comparable width in simulation bands for all three models. The similarity in these results is particularly notable given that estimation in this study differs from that in Cross et al. (2018) in four key ways: (1). the change in conditioning variable; (2). the change in fitting window; (3). the use of BLRP parameter estimators from the regression model given in Equation 5; and (4). the use of weighted quantile estimation across multiple climate model conditioned BLRP realisations.

The estimation of historical extremes at both sites is very good with all observations at Bochum falling within the weighted 95% simulation bands, and only one observation (the smallest) falling outside the simulation bands for Atherstone. At both gauges, and for all three BLRP model variants, the wQ50 provides very good estimation of the observed annual maxima up to approximately the 10-year return period rainfall event. For rarer events, the BL0 and BL1 models slightly underestimate the observed extremes, although the BL1M model performs better. At Atherstone, the wQ50 for the BL1M model estimates marginally higher extremes between the 10 and 100-year return periods than the BL0 and BL1 models. However, at Bochum, the BL1M model wQ50 accurately estimates the highest observed extreme. In comparison with the extreme rainfall estimation for the same sites and historical period in Cross et al. (2018), the mean estimation is very similar, although there is an increase in uncertainty represented by the 95% simulation bands. This increasing uncertainty is expected because the modelling framework in this study introduces climate and regression model uncertainty into estimation.

The estimation of future rainfall extremes under both climate warming scenarios – RCP 4.5 and 8.5 – shows a notable increase in rainfall amounts (cyan bold line for wQ50 and blue dashed lines for weighted 95 % simulation bands). Together with the increase in wQ50 extreme rainfall estimation for the two future

[2]The tabulated results are estimated from the nearest observed/simulated values with actual return periods of 9.4 and 93.1 years at Bochum, and 10.3 and 84.1 years at Atherstone. The difference in these return periods has arisen from the length of realisations but is considered to represent a sufficiently accurate estimate of the 10 and 100-year rainfall amounts at these gauge locations.

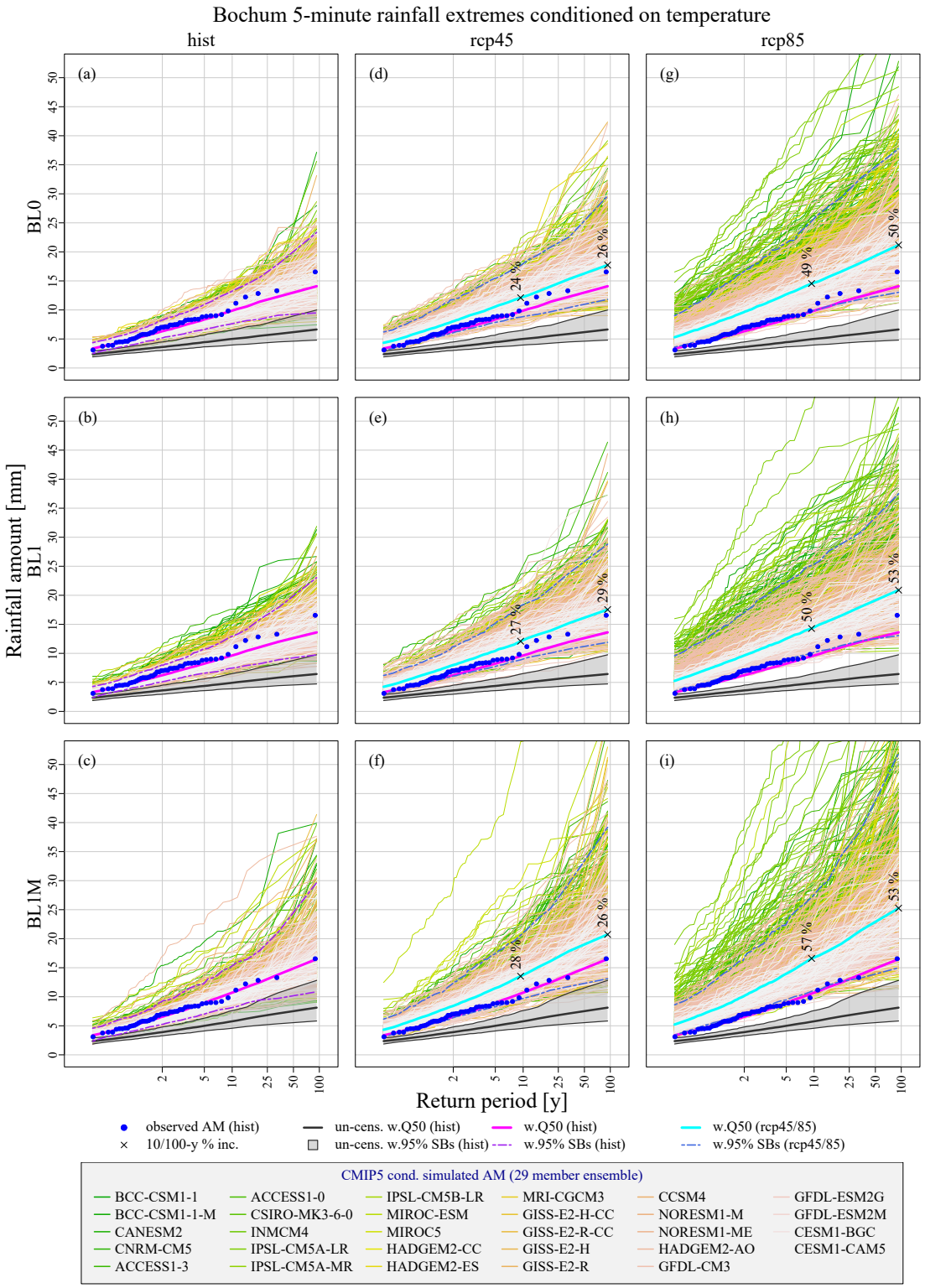


Figure 7: Estimation of 5-minute rainfall extremes at Bochum for historical and two future (2070-2100) climate warming scenarios, RCP4.5 and RCP8.5. Percentage values marked with crosses on the wQ50 lines (cyan) for future estimation shows the percentage increase in the wQ50 at the 10 and 100-year rainfall estimates compared with the historical.

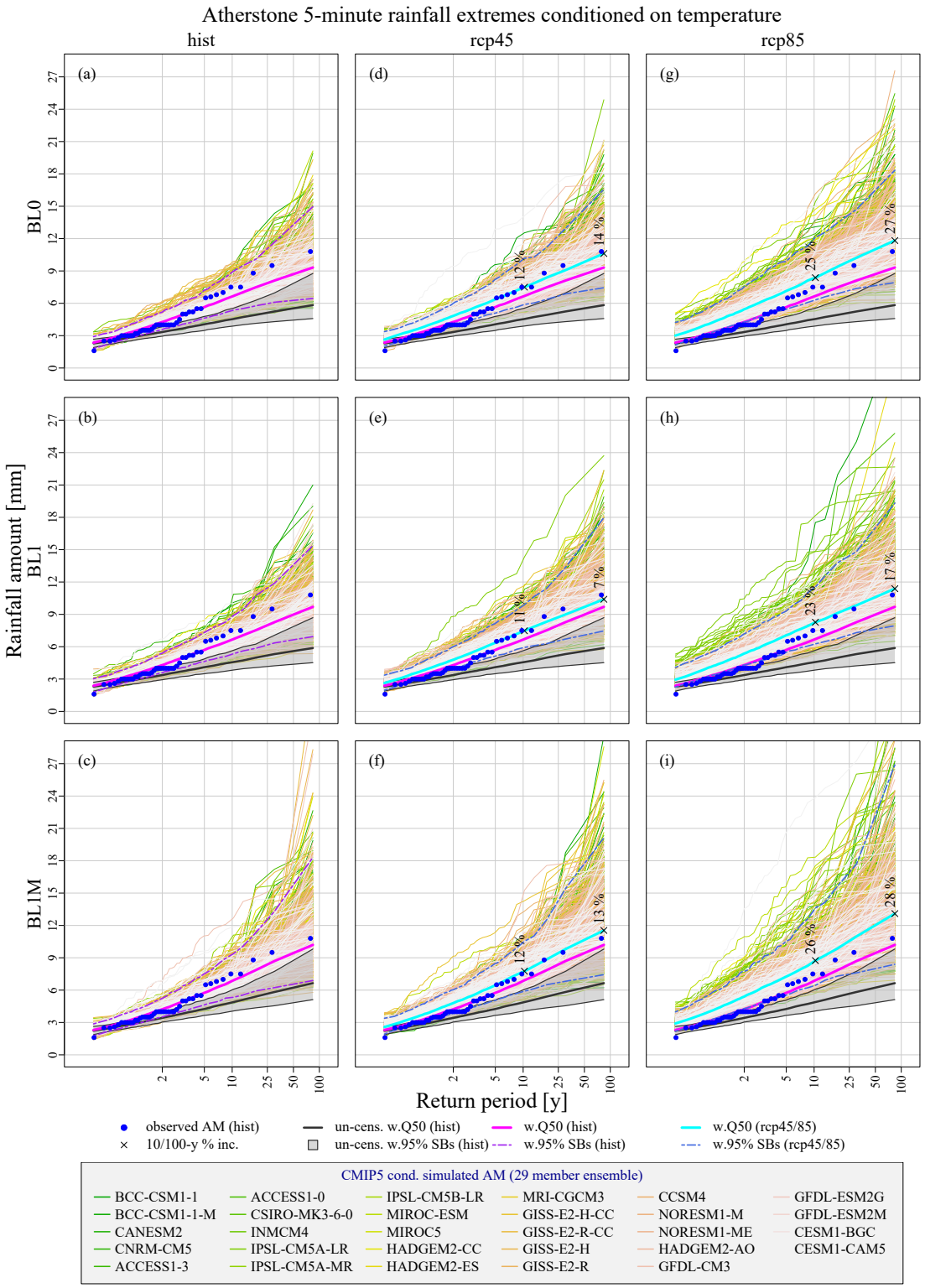


Figure 8: Estimation of 5-minute rainfall extremes at Atherstone for historical and two future (2070-2100) climate warming scenarios, RCP4.5 and RCP8.5. Percentage values marked with crosses on the wQ50 lines (cyan) for future estimation shows the percentage increase in the wQ50 at the 10 and 100-year rainfall estimates compared with the historical.

scenarios, there is a corresponding increase in the width of the simulation bands reflecting the increased error in estimation. The change in simulation band width is greater at Bochum than Atherstone. Given that the error in the fitted BLRP model parameter estimators is averaged across all new observations in the regression model, it is expected that the larger increase in simulation band widths at Bochum under the two climate change scenarios results from the regression uncertainty. This hypothesis is explored further in the discussion in Sect.7.

The greater expansion in simulation bands at Bochum than Atherstone may not be entirely unexpected because of the larger observed extremes in the historical period, and concomitant larger estimation in simulation bands. The growth in extremes at Bochum appears to be larger than that at Atherstone and hence the growth in simulation bands may also be expected to be faster than that at Atherstone. However, it can be seen from the extreme value plots for RCP 8.5 (Fig.7) that the extreme value realisations which fall outside the upper wQ97.5 simulation band for Bochum (predominantly green lines) are more spread out than those for Atherstone. This potentially indicates that one or several of the CMIP5 conditioned BLRP models (from the spectrum of greens in the legend) performs much worse in estimating the NCEP Q50 at Bochum than at Atherstone. This is reflected in the position of the wQ97.5 upper simulation band giving confidence that the weighting applied is beneficial in adjusting the position of the 95 % simulation bands in relation to all realizations. However, despite the use of weighted quantiles, the generation of so many highly divergent extreme value realizations will impact on the location of the wQ50 and wQ97.5. Given that the divergent extremes here are arising under RCP 8.5, it is necessary to investigate the range of extrapolation required for these models. This is discussed further in Sect.7.

## 7. Discussion

The results in Sect.6 show that the downscaling methodology set out in Sect.3 is successful at estimating rainfall extremes in the present climate, and has the flexibility to enable estimation in changed climates which are broadly in line with anticipated increases in local extremes of between 5-10 % per °C (see Precipitation Extremes in TFE.9, Cliamte Extremes in Stocker et al., 2013, p.112). Central to the downscaling approach is the regression model which enables anticipated changes in rainfall extremes to be estimated with simulation. Model validation has confirmed that the regression model parameters are effective at estimating the observed rainfall statistics, demonstrating that the models are well parameterised and that the rainfall generation process is robust. This gives credibility to the choice of regression model.

### *7.1. Limits on extrapolation*

In a warming climate, short duration extremes across Europe may become more prevalent with many more months within the year experiencing convective storm characteristic of summer months. This possible shift in rainfall pattern would be captured by the regression model on BLRP parameter estimators within the range of target covariate values thereby realising the increasing frequency of extremes. While more frequent summer storm events may increase the chance of higher intensity extremes, any notable increase in intensity is likely to arise from the extrapolation of BLRP parameter estimators for the hottest months in the year. Therefore, an important consideration in the estimation of rainfall extremes in any hypothesised warmer climate with the downscaling approach presented is the range of extrapolation.

Table 3 shows the maximum extrapolation in mean monthly near surface air temperature as a percentage of the target covariate range used in fitting for each CMIP5 conditioned BLRP model. Under RCP 4.5 there are a handful of models for which no extrapolation is required, numbers 18, 20, 26 and 27 at Bochum and numbers 1 and 2 at Atherstone. For all other models, some extrapolation is required for between 1 and 4 months of the year. Under RCP 8.5, some extrapolation is required for all CMIP5 conditioned BLRP models for at least 2 months of the year, and in some cases as many as 5 at Bochum and 4 at Atherstone.

The CMIP5 model requiring the maximum extrapolation, IPSL-CM5A-LR, falls within the green spectrum of models in Fig.7 and may be one of the models giving rise to the large number of very high extreme value realisations which fall outside the wQ97.5 upper simulation band in Fig.7. As highlighted in Sect.6, such divergent extremes can arise from poorly identified BLRP model parameters. Upon examination of

Table 3: Maximum extrapolation in mean monthly near surface air temperature as a percentage of the target covariate range required for simulation with each CMIP5 conditioned BLRP model (Ext [%]), and the number of months within the year (No. mons) for which extrapolation is needed for the two representative concentration pathways at each gauge location.

| | | Bochum | | | | Atherstone | | | |
|---|---|---|---|---|---|---|---|---|---|
| | | RCP 4.5 | | RCP 8.5 | | RCP 4.5 | | RCP 8.5 | |
| No. | CMIP5 model | Ext [%] | No. mons | Ext [%] | No. mons | Ext [%] | No. mons | Ext [%] | No. mons |
| 1 | bcc-csm1-1 | 4.4 | 1 | 41.2 | 4 | -0.9 | 0 | 20.2 | 3 |
| 2 | bcc-csm1-1-m | 4.5 | 2 | 24.1 | 3 | -1.5 | 0 | 17.2 | 2 |
| 3 | CanESM2 | 11.8 | 2 | 34.0 | 3 | 16.8 | 3 | 41.7 | 4 |
| 4 | CNRM-CM5 | 10.6 | 2 | 39.9 | 4 | 10.1 | 2 | 17.1 | 3 |
| 5 | ACCESS1-3 | 14.2 | 3 | 23.9 | 3 | 15.3 | 2 | 31.1 | 3 |
| 6 | ACCESS1-0 | 14.1 | 3 | 28.4 | 4 | 16.1 | 3 | 33.5 | 4 |
| 7 | CSIRO-Mk3-6-0 | 11.4 | 2 | 32.3 | 4 | 8.3 | 2 | 27.3 | 4 |
| 8 | inmcm4 | 9.0 | 1 | 14.6 | 2 | 11.3 | 1 | 19.4 | 3 |
| 9 | IPSL-CM5A-LR | 19.8 | 3 | 57.5 | 5 | 22.7 | 2 | 64.3 | 4 |
| 10 | IPSL-CM5A-MR | 18.4 | 2 | 26.6 | 3 | 11.6 | 1 | 22.1 | 2 |
| 11 | IPSL-CM5B-LR | 6.6 | 2 | 14.2 | 3 | 12.4 | 2 | 21.6 | 3 |
| 12 | MIROC-ESM | 18.9 | 3 | 27.4 | 3 | 24.1 | 3 | 36.4 | 4 |
| 13 | MIROC5 | 8.9 | 2 | 17.2 | 3 | 7.2 | 2 | 18.5 | 3 |
| 14 | HadGEM2-CC | 9.5 | 3 | 26.3 | 4 | 17.6 | 3 | 37.8 | 4 |
| 15 | HadGEM2-ES | 16.3 | 3 | 34.8 | 4 | 18.7 | 3 | 39.7 | 4 |
| 16 | MRI-CGCM3 | 0.2 | 1 | 7.8 | 2 | 3.8 | 1 | 14.3 | 2 |
| 17 | GISS-E2-H-CC | 7.8 | 2 | 15.3 | 3 | 7.2 | 2 | 15.7 | 3 |
| 18 | GISS-E2-R-CC | -0.7 | 0 | 7.6 | 2 | 3.3 | 1 | 11.8 | 2 |
| 19 | GISS-E2-H | 9.8 | 2 | 14.9 | 3 | 12.4 | 3 | 19.8 | 3 |
| 20 | GISS-E2-R | -0.2 | 0 | 6.3 | 2 | 3.2 | 2 | 11.8 | 2 |
| 21 | CCSM4 | 8.1 | 2 | 12.1 | 2 | 11.0 | 2 | 23.8 | 3 |
| 22 | NorESM1-M | 17.5 | 3 | 26.3 | 3 | 14.8 | 2 | 30.3 | 4 |
| 23 | NorESM1-ME | 14.1 | 3 | 25.4 | 4 | 12.9 | 3 | 26.0 | 4 |
| 24 | HadGEM2-AO | 19.7 | 4 | 37.2 | 5 | 22.2 | 4 | 40.3 | 4 |
| 25 | GFDL-CM3 | 24.9 | 3 | 42.0 | 4 | 35.0 | 4 | 52.5 | 4 |
| 26 | GFDL-ESM2G | -1.6 | 0 | 12.4 | 2 | 0.6 | 1 | 18.4 | 3 |
| 27 | GFDL-ESM2M | -1.8 | 0 | 5.5 | 2 | 6.7 | 2 | 16.7 | 3 |
| 28 | CESM1-BGC | 11.7 | 2 | 18.9 | 3 | 8.6 | 2 | 21.5 | 3 |
| 29 | CESM1-CAM5 | 10.0 | 2 | 19.3 | 3 | 14.0 | 2 | 31.1 | 4 |
| Mean extrapolation [%] | | 10.3 | - | 23.9 | - | 11.9 | - | 27.0 | - |
| Modal no. months | | - | 2 | - | 3 | - | 2 | - | 3 |

the parameter estimates for IPSL-CM5A-LR under RCPs 4.5 and 8.5, we find that the regression uncertainty grows very quickly for Bochum, indicating that the estimated parameters for high extrapolations are less well identified. Figure 9 shows the regressions on the IPSL-CM5A-LR conditioned BLRP estimators, together with the sampling ranges for MVN distributions of BLRP parameter estimators under RCPs 4.5 (blue hatched) and 8.5 (orange filled). The maximum extrapolation for sampling as a percentage of the target covariate range presented in Table 3 is shown in Fig.9 in the panels for the BLRP storm arrival rate parameter, $\lambda$ (a1, f1, k1, p1, u1, z1). The same percentages apply to all other plots but are not repeated.

We can see from Fig.9 that the regression uncertainty for two model parameters across each of the three BLRP model variants grow exponentially within the range of extrapolation under RCP 8.5 for Bochum: $\beta$ and $\gamma$ for BL0 (panels c1 and d1), and $\kappa$ and $\phi$ for BL1 (panels n1 and o1) and BL1M (panels x1 and y1). In each case we can see that the sampling range at the maximum extrapolation under RCP 8.5 is much wider than the same for RCP 4.5. With these wider confidence intervals, random sampling from

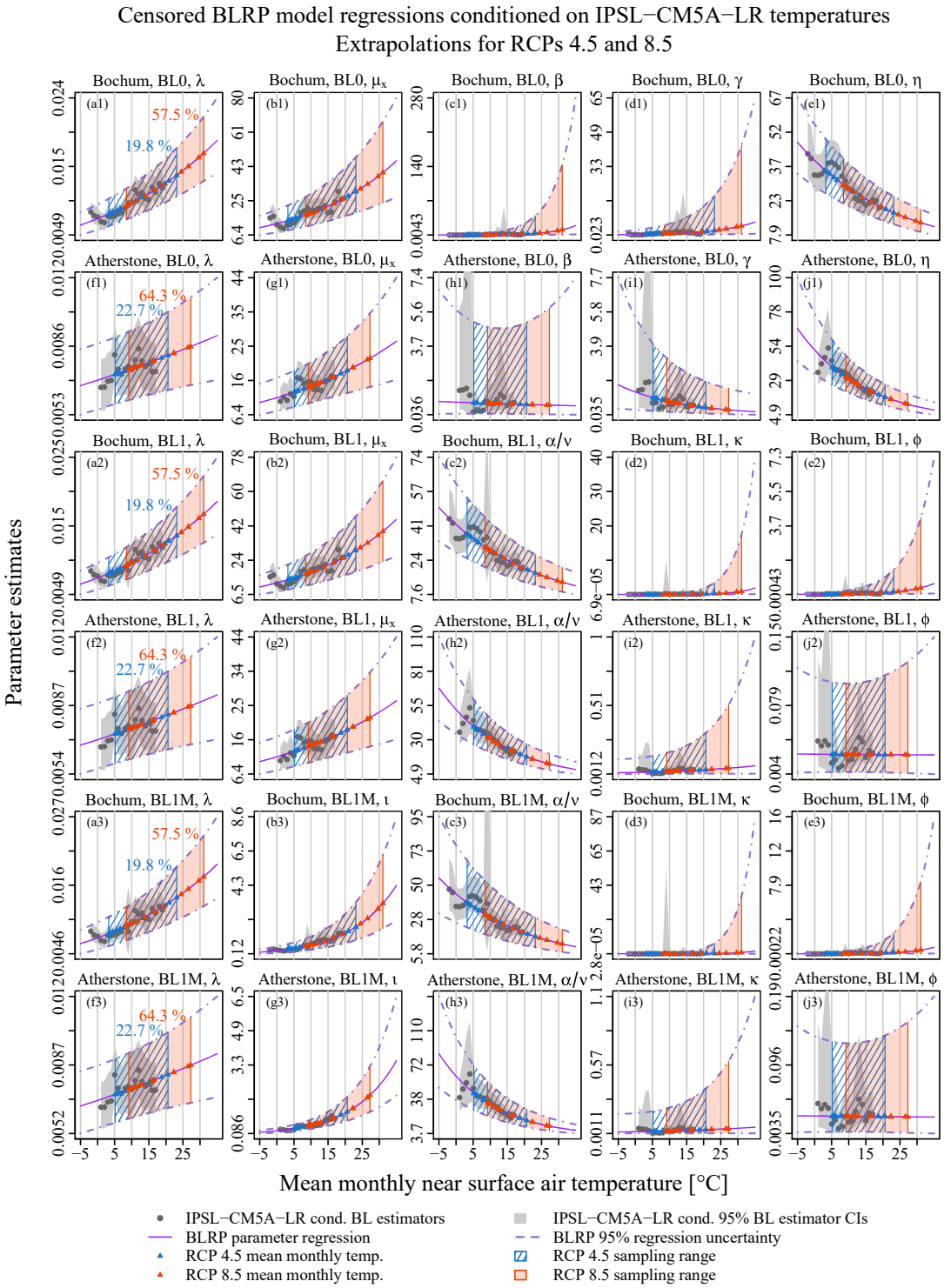


Figure 9: Regression extrapolation for BLRP parameter estimation under RCPs 4.5 and 8.5 showing the change in sampling range for the MVN distribution of BLRP parameter estimators.

the MVN distribution of BLRP parameter estimators will result in many parameter-sets which give rise to divergent extremes. This uncertainty is caused by the fit of the regression model to the fitted BLRP parameter estimators. Despite the greater extrapolation required for RCP 8.5 at Atherstone (64.3 %), the extreme value estimation in Fig.8 shows far fewer divergent extremes larger than the wQ97.5 upper simulation band for Atherstone, and it is not clear from the colour scale for the CMIP5 models whether those very high realisations are attributed to IPSL-CM5A-LR. However, we can see in Fig.10 that the regression uncertainty for Atherstone does not grow in the same way as it does for Bochum with higher mean monthly temperatures.

The example of the growth in regression uncertainties for the IPSL-CM5A-LR conditioned BLRP models at Bochum and Atherstone highlights an important limitation and potential source of criticism in the downscaling approach presented. That is one of using a regression for extrapolation beyond the range of the data used to fit it. In the context of estimating rainfall extremes in a climate warmer than today's using rainfall models, it is inevitable that the rainfall model parameters will require updating. The principal method for doing this is the delta change, or factor of change approach, which despite its own limitations (see discussion in Sect.2) avoids the issue of extrapolation. The primary concern with extrapolating regression models is the lack of knowledge about the shape the regression takes beyond the range of the data. In the model applied here, we have used simple linear regression on the natural logarithm of the fitted BLRP parameter estimators to capture their underlying relation with mean monthly near surface air temperature. While such a regression fails to match exactly the heterogeneity of individual estimators at different temperatures (see Figs.3 and 4), the high skill in the regression models to estimate rainfall extremes (Figs.7 and 8) and central moments of the rainfall time-series (Figs.5 and 6) in the present climate give confidence in the choice of the regression model.

On the assumption that the linear relations between model parameters and temperature are valid for increasing unobserved temperatures, and given that extrapolation is only required for between approximately 2-3 months of the year up to the most severe climate change projection, we feel that the model proposed is appropriate. However, because of the potential for rapid growth in the regression uncertainty demonstrated in the example of IPSL-CM5A-LR, it would be prudent to exercise caution in the use of downscaling based on regression. A simple and pragmatic approach is to set an upper limit on extrapolation for the most severe climate projection as a means of identifying a subset of climate models for simulation. In setting such a limit, a balance is sought between avoiding the rapid growth in regression uncertainties for some CMIP5 conditioned BLRP models and retaining valuable information regarding the nature of climate change projected by the climate models. If we leave out too many models from the ensemble which project higher changes in temperature than the others, we may underestimate the change in rainfall extremes.

Guided by the mean extrapolation across the complete ensemble of 29 CMIP5 models, 23.9 % for RCP 4.5 and 27 % for RCP 8.5 (see Table 3), we propose a limit of 30 %. At this limit, the ensemble member sizes reduce to 21 for Bochum and 18 for Atherstone. Upon removing these models, the number of extreme value realisations used for estimation reduces from 1160 to 840 at Bochum and 720 at Atherstone. These are still a considerable number of realisations at each location therefore no further realisations are simulated. Figure 10 shows the updated extreme rainfall estimation for the new ensembles at Bochum, and Table E.9 in Appendix E the updated 10 and 100 year estimated rainfall amounts corresponding to the plots in Fig.10. The new selections are listed in Table E.10 in Appendix E with new maximum extrapolations highlighted in red, and the mean extrapolation and modal number of months for which extrapolation is required updated.

Comparing the plots in Fig.10 with those in Fig.7, the change in Bochum extremes for RCP 4.5 is negligible following the removal of 8 ensemble members, although there is a noticeable change in the estimation of extremes for RCP 8.5. The extreme value realisations which exceed the wQ97.5 are more tightly concentrated around the upper band. This has resulted in a noticeable narrowing of the simulation bands for RCP 8.5, with the greatest change occurring in the location of the upper band. The reductions in wQ50 are marginal, but the reductions in simulation band widths are substantial and represent greater confidence in the estimation of extremes reflecting the greater confidence in the estimation of BLRP parameter estimators from the regression models.

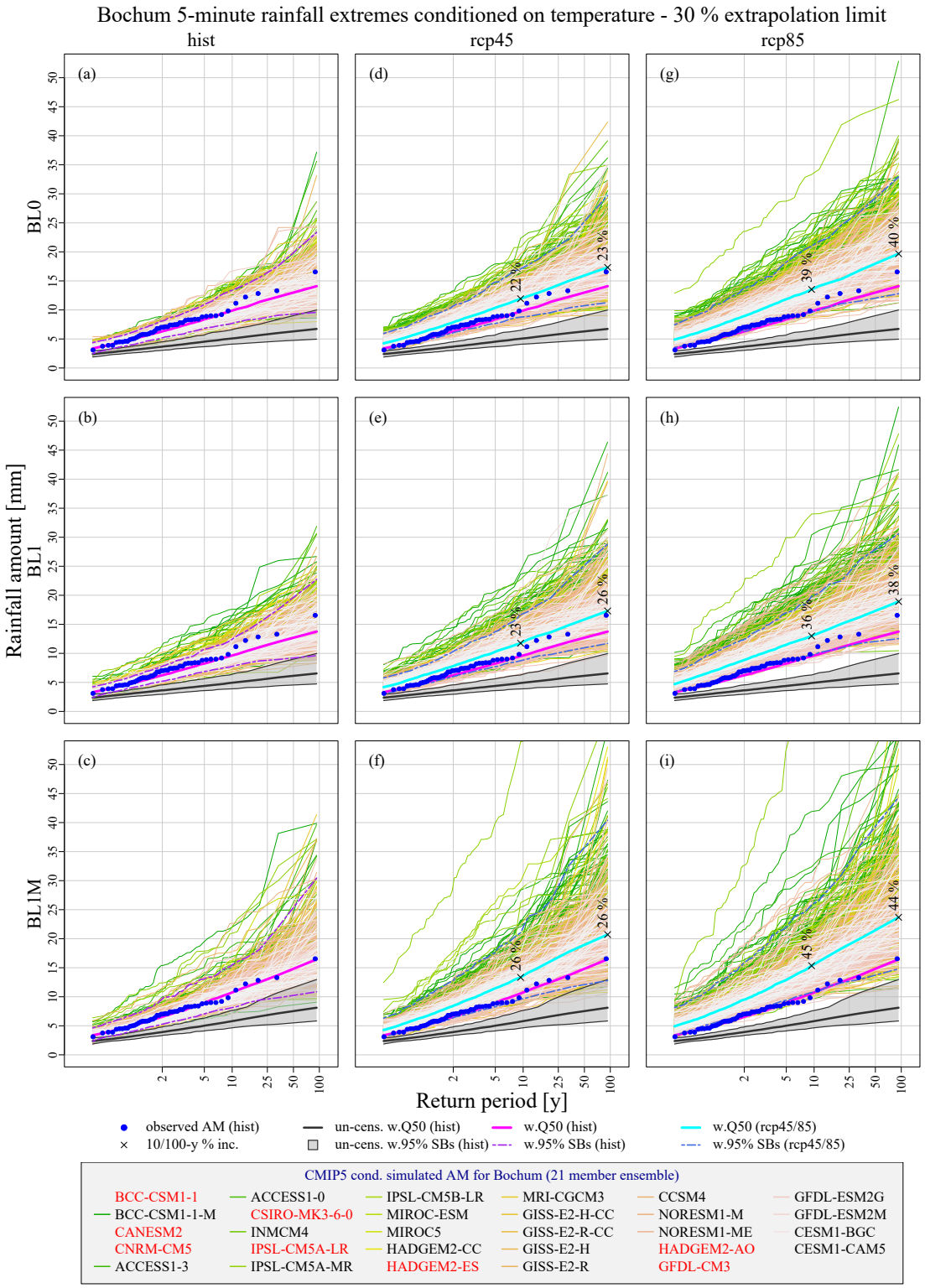


Figure 10: Extreme rainfall estimation at Bochum for historical and two future (2070-2100) climate warming scenarios, RCP4.5 and RCP8.5 with maximum limit of extrapolation for RCP 8.5 at 30 %. Climate models omitted from the estimation are highlighted red in the legend.

*7.2. Shift in simulation bands*

Fixing a limit on extrapolation has improved our confidence in the estimation of rainfall extremes at Bochum under RCP 8.5, although the total range of estimation has shifted marginally towards that of the present climate. While we are unable to validate estimates of future rainfall, it is useful to understand if those estimates are substantially different from those of the present climate. Figure 11 compares the range of extreme rainfall estimation at each location and climate forcing scenario with the estimation for the present climate. From a visual inspection of the plots in Fig.11, there is substantial overlap in estimation between sites and carbon forcing scenarios. This is particularly true at Atherstone under RCP 4.5 in which a very high proportion of the estimated future rainfall extremes are explained by the present-day estimation. Within the individual plots in Fig.11 are sub-plots giving the overlap of the simulation bands as a percentage for return period estimation between 2 and 100-years. The red dashed line gives the percentage of the historical estimation which overlaps the future. This may be interpreted as the percentage of the uncertainty in the current climate estimates which is still valid in the future.

The two primary observations from Fig.11 are that while the overlap in estimation increases for rarer events, it reduces for the more severe climate forcing scenario, RCP 8.5. These observations are intuitive and confirmed by the percentage values given in the sub-plots. With such substantial overlap at Atherstone under RCP 4.5, it may be argued that rainfall extremes are not expected to change under this climate forcing scenario up to the year 2100. However, at Bochum between approximately 35-55 % of future rainfall extremes are not estimated by the present climate, therefore we argue that extremes in this location are anticipated to change under RCP 4.5 between now and 2100. With between approximately 30-65 % of future extremes at Atherstone and 40-75 % at Bochum under RCP 8.5 not estimated by the current climate we again argue that extremes are expected to increase in both locations under this climate change scenario.

## 8. Conclusions

The downscaling methodology presented in this study offers a new approach for estimating rainfall extremes in a changing climate. It extends the censored modelling approach for short duration rainfall extremes presented in Cross et al. (2018) into a downscaling framework by changing the conditioning variable from calendar month which is discrete, to near surface air temperature which is continuous. While the change in conditioning variable is not new following the development of a local generalised method of moments fitting procedure by Kaczmarska et al. (2015), the modelling framework presented here is to the best of our knowledge the first to use multivariate linear regression to simultaneously estimate the full set of BLRP model parameter estimators.

In this research, it is hypothesised that mechanistic rainfall model parameters may be approximated by regression without significant detriment to rainfall simulation and the estimation of fine-scale extremes. This hypothesis is born out of the recognition that parameter estimators are dependent on the arbitrary selection of training data by calendar month or season. These selections are subjective and result in similar but varying parameterisations. The same effect is replicated in Fig.3 with the scatter plots for estimated parameters across all climate conditioned rainfall models. Because of the differences in simulated temperatures for the historical period from each climate model, the sampling of months in the rainfall record differs slightly giving rise to marginal variations in the estimated parameters. Despite this, we find that the resultant cloud of estimators for several model parameters follows an obvious dependence over narrow regions.

The objective of the regression model is to identify plausible regions in the parameter space within which well identified parameters can be sampled. To ensure the reliability of observations used to fit the regression model, a target covariate range for the conditioning covariate is identified based on a fixed K number of months. The good performance of the NCEP regression model in reproducing the fitting and validation statistics, and the skill with which extremes are estimated in the current climate using regressions fitted to all CMIP5 models, support the research hypothesis. These results also give confidence in the choice of regression model used.

A notable success of the downscaling methodology presented is the treatment of uncertainty. The simulation and estimation of extremes incorporates rainfall model uncertainty, the regression uncertainty, the

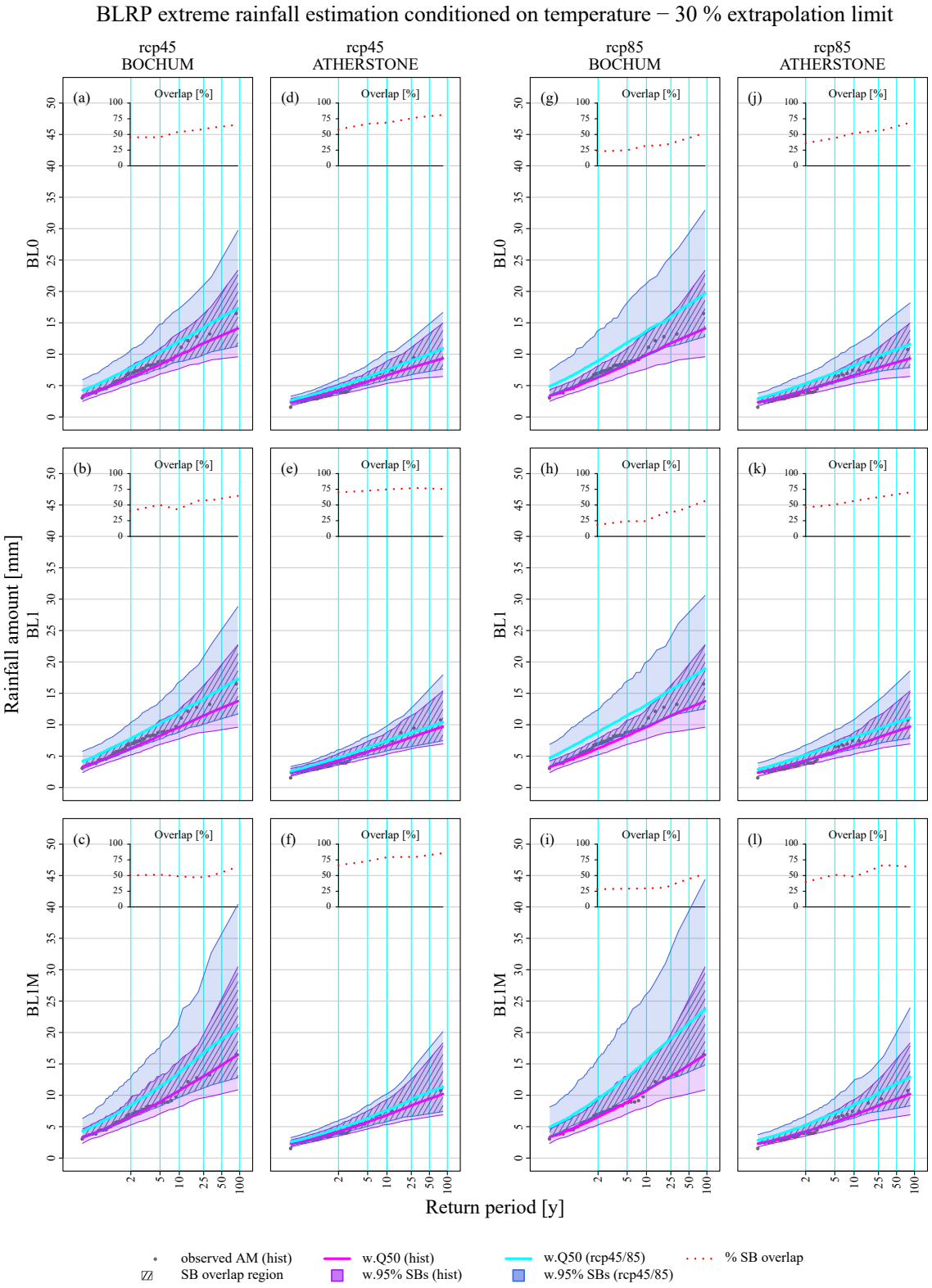


Figure 11: Overlap in the range of extreme rainfall estimation for Bochum and Atherstone under RCPs 4.5 and 8.5 with a 30 % limit applied to the maximum extrapolation under RCP 8.5.

sampling uncertainty of the stochastic process, and climate model uncertainty. The choice of prediction interval for the regression model uncertainty ensures that both the error in the position of the regression line and the variance of the observations around this are included. Climate model uncertainty is accounted for with the ensemble of CMIP5 climate model outputs and subsequent use of weighted quantiles to estimate simulation bands.

A limitation of the regression framework for downscaling is the potential for regression uncertainties to grow rapidly within the range of extrapolation required for more severe carbon forcing scenarios such as RCP8.5. In this study we find that the different regression fits for the two gauges investigated resulted in the generation of poorly identified parameter estimators under RCP 8.5 at Bochum, but well identified estimators at Atherstone. This raises the important issue of using regression models for extrapolation. A pragmatic solution is to place a limit on extrapolation and refine the CMIP5 climate model ensemble to include only those which fall below this limit. However, specifying a limit on extrapolation is difficult because the level of extrapolation required is a function of the target covariate range which itself is a function of the chosen K number of months, and the chosen increment between target values. Any imposed limit is also subjective.

A limit on extrapolation of 30 % was used at both gauge locations to mitigate the impact of parameter uncertainty on estimation, and to ensure that some climate conditioned rainfall models requiring above average extrapolation were retained. Despite this, extrapolation is only needed for between approximately 2 and 3 months in the year. Therefore, while the framework presented inevitably demands some extrapolation, we feel that the combination of inherent and imposed limitations mean that the required extrapolation is acceptable in the context of simulating rainfall in a changing climate.

The choice of temperature as the conditioning variable in this research was strongly influenced by the Clausius-Clapeyron relationship which explains the increase in atmospheric water vapour in a warming climate. Further research is required to investigate the relationship between BLRP parameter estimators and other covariates to provide extra validation of the approach, potentially with other model variants. Extension to multiple covariates would also enable the investigation of teleconnections such as the North Atlantic Oscillation which are known to influence European rainfall.

**Acknowledgements**

David Cross is grateful for the award of an Industrial Case Studentship from the Engineering and Physical Sciences Research Council (EPSRC) in the UK, and EDF Energy. David would like to acknowledge Pietro Bernardara who initiated his PhD with Christian Onof, but who has since taken up a new role at EDF in France. We are grateful to Clare Goodess of the University of East Anglia, Edward Pope of the UK Meteorological Office, and Nadarajah Ramesh of the University of Greenwich for their valuable insights in steering this research. We also thank the two anonymous referees and the editor for their constructive reviews and comments which have greatly improved this paper.

The Environment Agency of England is gratefully acknowledged for providing the UK rainfall data, and Deutsche Montan Technologie and Emschergenossenschaft / Lippeverband in Germany are gratefully acknowledged for providing the Bochum data.

We acknowledge the World Climate Research Programme's Working Group on Coupled Modelling, which is responsible for CMIP, and we thank the climate modelling groups (listed in Table B.5 in Appendix B of this paper) for producing and making available their model outputs. For CMIP, the U.S. Department of Energy's Program for Climate Model Diagnosis and Intercomparison provided coordinating support and led development of software infrastructure in partnership with the Global Organization for Earth System Science Portals. The NCEP Reanalysis data were provided by the NOAA/OAR/ESRL PSD, Boulder, Colorado, USA, from their website at https://www.esrl.noaa.gov/psd/.

## Appendix A. Bartlett-Lewis model parameters

Table A.4: Model parameters for original and randomised BLRP models.

| **Description** | **Units** | **BL0** | **BL1** | **BL1M** |
|---|---|---|---|---|
| Storm arrival rate | $\mathrm{hr}^{-1}$ | $\lambda$ | $\lambda$ | $\lambda$ |
| Cell arrival rate | $\mathrm{hr}^{-1}$ | $\beta$ | $\{\beta\}$[1] | $\{\beta\}$ |
| Ratio of cell arrival rate to cell duration | - | - | $\kappa = \{\beta/\eta\}$ | $\kappa = \{\beta/\eta\}$ |
| Mean cell depth | $\mathrm{mmhr}^{-1}$ | $\mu_x$ | $\mu_x$ | $\{\mu_x\}$ |
| Ratio of mean cell depth to cell duration | mm | - | - | $\iota = \{\mu_x/\eta\}$ |
| Ratio of standard deviation to the mean cell depth | - | $r = \sigma_x/\mu_x$ | $r = \sigma_x/\mu_x$ | $r = \sigma_x/\mu_x$ |
| Expected square of the cell depth[2] | $\mathrm{mm}^2\mathrm{hr}^{-2}$ | $[\mu_{x^2}]$ | $[\mu_{x^2}]$ | $[\mu_{x^2}]$ |
| Expected cube of the cell depth for inclusion of skewness in the objective function[2] | $\mathrm{mm}^3\mathrm{hr}^{-3}$ | $[\mu_{x^3}]$ | $[\mu_{x^3}]$ | $[\mu_{x^3}]$ |
| Cell duration parameter | $\mathrm{hr}^{-1}$ | $\eta$ | $\{\eta\}$ | $\{\eta\}$ |
| Gamma scale parameter for $\eta$ | hr | - | $\nu$ | $\nu$ |
| Gamma shape parameter for $\eta$ | - | - | $\alpha$ | $\alpha$ |
| Storm duration parameter | $\mathrm{hr}^{-1}$ | $\gamma$ | $\{\gamma\}$ | $\{\gamma\}$ |
| Ratio of storm duration to cell duration | - | - | $\phi = \{\gamma/\eta\}$ | $\phi = \{\gamma/\eta\}$ |
| Number of parameters: exponential cell intensity[3] | - | 5 | 6 | 6 |
| Number of parameters: gamma cell intensity[3] | - | 6 | 7 | 7 |

1. Letters appearing in curly brackets {..} refer to random variables that are not model parameters but are randomisations of model parameters in previous models.
2. For the two parameter gamma cell depth distribution, the expected square and cube of the cell depth ($\mu_{x^2}$ and $\mu_{x^3}$, shown in square [..] brackets) are calculated from the standard deviation ($\sigma_x$) and mean ($\mu_x$) of the cell depth. In practice it is the ratio of these (r) which is parameterized enabling calculation of $\mu_{x^2}$ and $\mu_{x^3}$. For both the exponential and gamma distributions, $\mu_{x^2} = f_1{\mu_x}^2$ and $\mu_{x^3} = f_2{\mu_x}^3$ where $f_1 = 1+r^2$ and $f_2 = 1+3r^2+2r^4$. Because the exponential distribution is a special case of the gamma distribution where r is equal to 1, $\mu_{x^2} = 2{\mu_x}^2$ and $\mu_{x^3} = 6{\mu_x}^3$. Therefore it is not necessary to parameterize r for the exponential distribution, meaning the exponential versions of these models require 1 parameter less with r set to 1 in calibration.
3. If $\alpha$ is held fixed, the number of parameters to be calibrated for the randomised versions of the models (BL1 and BL1M) reduces by 1.

## Appendix B. Climate model data

Table B.5: List of models used in the downscaling experiment. Information on model type and components is adapted from IPCC AR5 report The Physical Science Basis Chapter 9, Appendix A Flato et al. (2013). The reader is referred to this Appendix for the principal references of the individual climate models.

Start of Table B.5

| Modelling group | Model name | Model type [1] |
|---|---|---|
| BCC (Beijing Climate Center, China Meteorological Administration) | (1). bcc-csm1.1 | (1). ES |
| | (2). bcc-csm1-1-m | (2). ES |
| CCCma (Canadian Centre for Climate Modelling and Analysis) | (3). CanESM2 | (3). ES |
| CNRM-CERFACS (Centre National de Recherches Météorologiques and Centre Europeen de Recherche et Formation Avancees en Calcul Scientifique, France) | (4). CNRM-CM5 | (4). ES |
| CSIRO-BOM (Commonwealth Scientific and Industrial Research Organisation and Bureau of Meteorology, Australia) | (5). ACCESS1.0 | (5). ES |
| | (6). ACCESS1.3 | (6). ES |
| CSIRO-QCCCE (Commonwealth Scientific and Industrial Research Organisation and Queensland Climate Change Centre of Excellence, Australia) | (7). CSIRO-Mk3-6-0 | (7). AO |
| INM (Institute for Numerical Mathematics, Russia) | (8). INM-CM4 | (8). ES |
| IPSL (Institut Pierre-Simon Laplace, France) | (9). IPSL-CM5A-LR | (9). ES |
| | (10). IPSL-CM5A-MR | (10). ES |
| | (11). IPSL-CM5B-LR | (11). ES |
| MIROC (Model for Interdisciplinary Research on Climate, University of Tokyo, National Institute for Environmental Studies, and Japan Agency for Marine-Earth Science and Technology) | (12). MIROC-ESM | (12). ES |
| | (13). MIROC5 | (13). AO |
| MOHC (Meteorological Office Hadley Centre, UK) | (14). HadGEM2-CC | (14). ES |
| | (15). HadGEM2-ES | (15). ES |
| MRI (Meteorological Research Institute, Japan Meteorological Agency) | (16). MRI-CGCM3 | (16). AO |
| NASA-GISS (National Aeronautics and Space Administration, Goddard Institute for Space Studies, USA) | (17). GISS-E2-H-CC | (17). ES |
| | (18). GISS-E2-R-CC | (18). ES |
| | (19). GISS-E2-H | (19). AO |
| | (20). GISS-E2-R | (20). AO |
| NCAR (National Centre for Atmospheric Research, USA) | (21). CCSM4 | (21). AO |
| NCC (Norwegian Climate Centre) | (22). NorESM1-M | (22). ES |
| | (23). NorESM1-ME | (23). ES |
| NIMR-KMA (National Institute of Meteorological Research, Korea Meteorological Administration) | (24). HadGEM2-AO | (24). AO |

Continuation of Table B.5

| Modelling group | Model name | Model type [1] |
|---|---|---|
| NOAA-GFDL (National Oceanic and Atmospheric Administration, Geophysical Fluid Dynamics Laboratory, USA) | (25). GFDL-CM3<br>(26). GFDL-ESM2G<br>(27). GFDL-ESM2M | (25). AO<br>(26). ES<br>(27). ES |
| NSF-DOE-NCAR (National Science Foundation; US Department of Energy; National Centre for Atmospheric Research, USA) | (28). CESM1(BGC)<br>(29). CESM1-CAM5 | (28). ES<br>(29). ES |

End of Table B.5

1. Model types are broadly categorised as: AO (coupled atmosphere-ocean global circulation models) and ES (earth system models).

## Appendix C. Bartlett-Lewis regression model statistics

Table C.6: Censored BLRP model regression coefficients conditioned on NCEP mean monthly near surface air temperatures and associated analysis of variance (ANOVA) summary statistics.

| BL0 | | $\ln(\lambda)$ $\ln[h^{-1}]$ | $\ln(\mu_x)$ $\ln[mmh^{-1}]$ | $\ln(\beta)$ $\ln[h^{-1}]$ | $\ln(\gamma)$ $\ln[h^{-1}]$ | $\ln(\eta)$ $\ln[h^{-1}]$ |
|---|---|---|---|---|---|---|
| Bochum | $b_0$ | -5.0016 | 2.3977 | -1.8602 | -0.7653 | 3.8356 |
| | $b_p$ | 0.0315 | 0.0499 | 0.0894 | 0.0269 | -0.0456 |
| | $R^2$ | 0.8292 | 0.7941 | 0.3068 | 0.0384 | 0.8171 |
| | F-stat | 87.4022 | 69.4377 | 7.9671 | 0.7184 | 80.4031 |
| | $P(>F)$ | $2.5 \times 10^{-8}$ | $1.4 \times 10^{-7}$ | 0.0113 | 0.4078 | $4.7 \times 10^{-8}$ |
| Atherstone | $b_0$ | -5.049 | 2.1371 | -0.4424 | 0.3696 | 4.1029 |
| | $b_p$ | 0.0186 | 0.0515 | 0.005 | -0.0509 | -0.0556 |
| | $R^2$ | 0.4762 | 0.8136 | 0.001 | 0.1218 | 0.7083 |
| | F-stat | 10.9114 | 52.3724 | 0.0114 | 1.665 | 29.1421 |
| | $P(>F)$ | 0.0063 | $1.0 \times 10^{-5}$ | 0.9166 | 0.2212 | 0.0002 |
| BL1 | | $\ln(\lambda)$ $\ln[h^{-1}]$ | $\ln(\mu_x)$ $\ln[mmh^{-1}]$ | $\ln(\alpha/\nu)$ $\ln[h^{-1}]$ | $\ln(\kappa)$ $[-]$ | $\ln(\phi)$ $[-]$ |
| Bochum | $b_0$ | -4.9914 | 2.4035 | 3.8635 | -5.6943 | -4.6006 |
| | $b_p$ | 0.0316 | 0.0481 | -0.0455 | 0.1408 | 0.0762 |
| | $R^2$ | 0.8262 | 0.7292 | 0.8108 | 0.4834 | 0.2391 |
| | F-stat | 85.549 | 48.4587 | 77.1301 | 16.8413 | 5.6550 |
| | $P(>F)$ | $2.9 \times 10^{-8}$ | $1.7 \times 10^{-6}$ | $6.3 \times 10^{-8}$ | 0.0007 | 0.0287 |
| Atherstone | $b_0$ | -5.0391 | 2.1466 | 4.1333 | -4.5414 | -3.7318 |
| | $b_p$ | 0.0186 | 0.051 | -0.056 | 0.0605 | 0.0048 |
| | $R^2$ | 0.477 | 0.8091 | 0.7078 | 0.1352 | 0.0014 |
| | F-stat | 10.9429 | 50.8532 | 29.068 | 1.8753 | 0.0171 |
| | $P(>F)$ | 0.0062 | $1.2 \times 10^{-5}$ | 0.0002 | 0.1959 | 0.8981 |
| BL1M | | $\ln(\lambda)$ $\ln[h^{-1}]$ | $\ln(\iota)$ $\ln[mm]$ | $\ln(\alpha/\nu)$ $\ln[h^{-1}]$ | $\ln(\kappa)$ $[-]$ | $\ln(\phi)$ $[-]$ |
| Bochum | $b_0$ | -4.9993 | -1.4339 | 3.9648 | -5.7987 | -4.6619 |
| | $b_p$ | 0.0321 | 0.0953 | -0.0524 | 0.1453 | 0.0846 |
| | $R^2$ | 0.802 | 0.8905 | 0.8132 | 0.4872 | 0.2609 |
| | F-stat | 72.9159 | 146.4254 | 78.3788 | 17.0984 | 6.3544 |
| | $P(>F)$ | $9.6 \times 10^{-8}$ | $4.4 \times 10^{-10}$ | $5.6 \times 10^{-8}$ | 0.0006 | 0.0214 |
| Atherstone | $b_0$ | -5.0564 | -1.983 | 4.2999 | -4.4155 | -3.6628 |
| | $b_p$ | 0.0188 | 0.1085 | -0.065 | 0.0552 | 0.0036 |
| | $R^2$ | 0.4942 | 0.9397 | 0.698 | 0.1004 | 0.0007 |
| | F-stat | 11.7254 | 187.0202 | 27.7369 | 1.3395 | 0.0084 |
| | $P(>F)$ | 0.0050 | $1.1 \times 10^{-8}$ | 0.0002 | 0.2696 | 0.9283 |

## Appendix D. Supplementary material to Sect.6

Table D.7: Bochum 10 and 100-year return period weighted extreme rainfall estimates [mm] for the historical and two future (2070-2100) climate warming scenarios, RCP 4.5 and 8.5 corresponding to the plots in Fig.7. Return period estimates are based on the nearest observed/simulated values with actual estimated return periods of 9.4 and 93.1 years. SB refers to Simulation Band.

| | Historical | | RCP4.5 | | RCP8.5 | |
|---|---|---|---|---|---|---|
| **BL0** | **10-yr** | **100-yr** | **10-yr** | **100-yr** | **10-yr** | **100-yr** |
| wQ2.5 | 7.5 | 9.5 | 8.8 | 11.8 | 9.8 | 13.0 |
| wQ50 | 9.7 | 14.1 | 12.1 | 17.7 | 14.5 | 21.2 |
| wQ97.5 | 13.0 | 23.3 | 17.6 | 29.6 | 25.3 | 37.8 |
| SB widths | 5.5 | 13.8 | 8.8 | 17.8 | 15.5 | 24.8 |
| SB widths increase (%) | - | - | 60 | 29 | 182 | 80 |
| **BL1** | **10-yr** | **100-yr** | **10-yr** | **100-yr** | **10-yr** | **100-yr** |
| wQ2.5 | 7.4 | 9.7 | 8.9 | 11.9 | 10.0 | 13.1 |
| wQ50 | 9.5 | 13.6 | 12.1 | 17.5 | 14.3 | 20.9 |
| wQ97.5 | 12.8 | 23.0 | 18.2 | 28.8 | 25.1 | 37.5 |
| SB widths | 5.4 | 13.3 | 9.3 | 16.9 | 15.1 | 24.4 |
| SB widths increase (%) | - | - | 72 | 27 | 180 | 83 |
| **BL1M** | **10-yr** | **100-yr** | **10-yr** | **100-yr** | **10-yr** | **100-yr** |
| wQ2.5 | 8.0 | 10.9 | 9.6 | 13.1 | 10.9 | 15.0 |
| wQ50 | 10.5 | 16.5 | 13.5 | 20.7 | 16.6 | 25.3 |
| wQ97.5 | 15.0 | 29.7 | 20.6 | 39.2 | 27.1 | 51.9 |
| SB widths | 7.0 | 18.8 | 11.0 | 26.1 | 16.2 | 36.9 |
| SB widths increase (%) | - | - | 57 | 39 | 131 | 96 |

Table D.8: Atherstone 10 and 100-year return period weighted extreme rainfall estimates [mm] for the historical and two future (2070-2100) climate warming scenarios, RCP 4.5 and 8.5 corresponding to the plots in Fig.7. Return period estimates are based on the nearest observed/simulated values with actual estimated return periods of 10.3 and 84.1 years. SB refers to Simulation Band.

| | Historical | | RCP4.5 | | RCP8.5 | |
|---|---|---|---|---|---|---|
| **BL0** | **10-yr** | **100-yr** | **10-yr** | **100-yr** | **10-yr** | **100-yr** |
| wQ2.5 | 5.4 | 6.5 | 5.9 | 7.4 | 6.3 | 7.9 |
| wQ50 | 6.7 | 9.3 | 7.5 | 10.6 | 8.4 | 11.8 |
| wQ97.5 | 9.0 | 15.0 | 10.2 | 16.6 | 12.1 | 18.3 |
| SB widths | 3.6 | 8.5 | 4.3 | 9.2 | 5.8 | 10.4 |
| SB widths increase (%) | - | - | 19 | 8 | 61 | 22 |
| **BL1** | **10-yr** | **100-yr** | **10-yr** | **100-yr** | **10-yr** | **100-yr** |
| wQ2.5 | 5.4 | 6.9 | 5.9 | 7.5 | 6.3 | 7.9 |
| wQ50 | 6.7 | 9.7 | 7.5 | 10.4 | 8.3 | 11.4 |
| wQ97.5 | 8.9 | 15.4 | 9.9 | 18.0 | 11.5 | 19.3 |
| SB widths | 3.5 | 8.5 | 4.0 | 10.5 | 5.2 | 11.4 |
| SB widths increase (%) | - | - | 14 | 24 | 49 | 34 |
| **BL1M** | **10-yr** | **100-yr** | **10-yr** | **100-yr** | **10-yr** | **100-yr** |
| wQ2.5 | 5.3 | 6.9 | 5.9 | 7.4 | 6.4 | 8.4 |
| wQ50 | 6.9 | 10.2 | 7.8 | 11.5 | 8.7 | 13.1 |
| wQ97.5 | 9.4 | 18.3 | 10.5 | 20.1 | 13.6 | 26.9 |
| SB widths | 4.1 | 11.4 | 4.6 | 12.7 | 7.2 | 18.5 |
| SB widths increase (%) | - | - | 12 | 11 | 76 | 62 |

## Appendix E. Supplementary material to Sect.7

Table E.9: Bochum 10 and 100-year return period weighted extreme rainfall estimates [mm] for the historical and two future (2070-2100) climate warming scenarios, RCP 4.5 and 8.5 with a maximum limit on extrapolation for RCP 8.5 of 30 %.

| | Historical | | RCP4.5 | | RCP8.5 | |
|---|---|---|---|---|---|---|
| **BL0** | **10-yr** | **100-yr** | **10-yr** | **100-yr** | **10-yr** | **100-yr** |
| wQ2.5 | 7.6 | 9.6 | 8.8 | 11.3 | 9.6 | 12.8 |
| wQ50 | 9.7 | 14.1 | 11.9 | 17.3 | 13.5 | 19.7 |
| wQ97.5 | 13.2 | 23.3 | 17.1 | 29.7 | 21.0 | 32.9 |
| SB widths | 5.6 | 13.7 | 8.3 | 18.4 | 11.4 | 20.1 |
| **BL1** | **10-yr** | **100-yr** | **10-yr** | **100-yr** | **10-yr** | **100-yr** |
| wQ2.5 | 7.6 | 9.6 | 8.7 | 11.7 | 9.7 | 12.5 |
| wQ50 | 9.5 | 13.8 | 11.7 | 17.3 | 13.0 | 18.9 |
| wQ97.5 | 12.1 | 22.7 | 16.6 | 28.8 | 19.8 | 30.6 |
| SB widths | 4.5 | 13.1 | 7.9 | 17.1 | 10.1 | 18.1 |
| **BL1M** | **10-yr** | **100-yr** | **10-yr** | **100-yr** | **10-yr** | **100-yr** |
| wQ2.5 | 8.0 | 10.9 | 9.6 | 12.8 | 10.7 | 14.8 |
| wQ50 | 10.6 | 16.5 | 13.3 | 20.7 | 15.3 | 23.7 |
| wQ97.5 | 15.2 | 30.5 | 21.0 | 40.4 | 25.8 | 44.3 |
| SB widths | 7.2 | 19.6 | 11.4 | 27.6 | 15.1 | 29.5 |

Table E.10: Maximum extrapolation in mean monthly near surface air temperature as a percentage of the target covariate range for a selection of CMIP5 climate models with a maximum limit on extrapolation for RCP 8.5 of 30 %. The ensemble of climate models has reduced to 21 for Bochum, and 18 for Atherstone.

| | | Bochum | | | | Atherstone | | | |
|---|---|---|---|---|---|---|---|---|---|
| | | RCP 4.5 | | RCP 8.5 | | RCP 4.5 | | RCP 8.5 | |
| No. | CMIP5 model | Ext [%] | No. mons | Ext [%] | No. mons | Ext [%] | No. mons | Ext [%] | No. mons |
| 1 | bcc-csm1-1 | - | - | - | - | -0.9 | 0 | 20.2 | 3 |
| 2 | bcc-csm1-1-m | 4.5 | 2 | 24.1 | 3 | -1.5 | 0 | 17.2 | 2 |
| 3 | CanESM2 | - | - | - | - | - | - | - | - |
| 4 | CNRM-CM5 | - | - | - | - | 10.1 | 2 | 17.1 | 3 |
| 5 | ACCESS1-3 | 14.2 | 3 | 23.9 | 3 | - | - | - | - |
| 6 | ACCESS1-0 | 14.1 | 3 | 28.4 | 4 | - | - | - | - |
| 7 | CSIRO-Mk3-6-0 | - | - | - | - | 8.3 | 2 | 27.3 | 4 |
| 8 | inmcm4 | 9.0 | 1 | 14.6 | 2 | 11.3 | 1 | 19.4 | 3 |
| 9 | IPSL-CM5A-LR | - | - | - | - | - | - | - | - |
| 10 | IPSL-CM5A-MR | 18.4 | 2 | 26.6 | 3 | 11.6 | 1 | 22.1 | 2 |
| 11 | IPSL-CM5B-LR | 6.6 | 2 | 14.2 | 3 | 12.4 | 2 | 21.6 | 3 |
| 12 | MIROC-ESM | 18.9 | 3 | 27.4 | 3 | - | - | - | - |
| 13 | MIROC5 | 8.9 | 2 | 17.2 | 3 | 7.2 | 2 | 18.5 | 3 |
| 14 | HadGEM2-CC | 9.5 | 3 | 26.3 | 4 | - | - | - | - |
| 15 | HadGEM2-ES | - | - | - | - | - | - | - | - |
| 16 | MRI-CGCM3 | 0.2 | 1 | 7.8 | 2 | 3.8 | 1 | 14.3 | 2 |
| 17 | GISS-E2-H-CC | 7.8 | 2 | 15.3 | 3 | 7.2 | 2 | 15.7 | 3 |
| 18 | GISS-E2-R-CC | -0.7 | 0 | 7.6 | 2 | 3.3 | 1 | 11.8 | 2 |
| 19 | GISS-E2-H | 9.8 | 2 | 14.9 | 3 | 12.4 | 3 | 19.8 | 3 |
| 20 | GISS-E2-R | -0.2 | 0 | 6.3 | 2 | 3.2 | 2 | 11.8 | 2 |
| 21 | CCSM4 | 8.1 | 2 | 12.1 | 2 | 11.0 | 2 | 23.8 | 3 |
| 22 | NorESM1-M | 17.5 | 3 | 26.3 | 3 | - | - | - | - |
| 23 | NorESM1-ME | 14.1 | 3 | 25.4 | 4 | 12.9 | 3 | 26.0 | 4 |
| 24 | HadGEM2-AO | - | - | - | - | - | - | - | - |
| 25 | GFDL-CM3 | - | - | - | - | - | - | - | - |
| 26 | GFDL-ESM2G | -1.6 | 0 | 12.4 | 2 | 0.6 | 1 | 18.4 | 3 |
| 27 | GFDL-ESM2M | -1.8 | 0 | 5.5 | 2 | 6.7 | 2 | 16.7 | 3 |
| 28 | CESM1-BGC | 11.7 | 2 | 18.9 | 3 | 8.6 | 2 | 21.5 | 3 |
| 29 | CESM1-CAM5 | 10.0 | 2 | 19.3 | 3 | - | - | - | - |
| Mean extrapolation [%] | | 8.5 | - | 17.8 | - | 7.1 | - | 19.1 | - |
| Modal no. months | | - | 2 | - | 3 | - | 2 | - | 3 |

## References


Abdellatif M, Atherton W, Alkhaddar R. Application of the stochastic model for temporal rainfall disaggregation for hydrological studies in north western england. Journal of Hydroinformatics 2013;15(2):555–67. PT: J; NR: 19; TC: 3; J9: J HYDROINFORM; PG: 13; GA: 124QY; UT: WOS:000317481900024.

Ailliot P, Allard D, Monbet V, Naveau P. Stochastic weather generators: an overview of weather type models 2014;.

Ali H, Mishra V. Contrasting response of rainfall extremes to increase in surface air and dewpoint temperatures at urban locations in india. Scientific Reports 2017;7(1):1228.

Arnbjerg-Nielsen K. Past, present, and future design of urban drainage systems with focus on danish experiences. Water Science and Technology 2011;63(3):527–35.

Bordoy R, Burlando P. Stochastic downscaling of climate model precipitation outputs in orographically complex regions: 2. downscaling methodology. Water Resources Research 2014a;50(1):562–79.

Bordoy R, Burlando P. Stochastic downscaling of precipitation to high-resolution scenarios in orographically complex regions: 1. model evaluation. Water Resources Research 2014b;50(1):540–61.

Bárdossy A, Plate EJ. Space-time model for daily rainfall using atmospheric circulation patterns. Water Resources Research 1992;28(5):1247–59.

Bárdossy A, Stehlík J, Caspary HJ. Automated objective classification of daily circulation patterns for precipitation and temperature downscaling based on optimized fuzzy rules. Climate Research 2002;23(1):11–22.

Burlando P, Rosso R. Extreme storm rainfall and climatic change. Atmospheric Research 1991;27(1-3):169–89.

Burton A, Fowler H, Blenkinsop S, Kilsby C. Downscaling transient climate change using a neyman–scott rectangular pulses stochastic rainfall model. Journal of Hydrology 2010;381(1):18–32.

Burton A, Kilsby CG, Fowler H, Cowpertwait P, O'connell P. Rainsim: A spatial–temporal stochastic rainfall modelling system. Environmental Modelling & Software 2008;23(12):1356–69.

Chandler R, Lourmas G, Jesus J. MOMFIT Software for moment-based fitting of single-site stochastic rainfall model fitting, User guide. Technical Report; Department of Statistical Science, University College London; 2010.

Cross D, Onof C, Winter H, Bernardara P. Censored rainfall modelling for estimation of fine-scale extremes. Hydrology and Earth System Sciences 2018;22(1):727.

Debele B, Srinivasan R, Parlange JY. Accuracy evaluation of weather data generation and disaggregation methods at finer timescales. Advances in Water Resources 2007;30(5):1286–300.

Evin G, Favre AC. Further developments of a transient poisson-cluster model for rainfall. Stochastic environmental research and risk assessment 2013;27(4):831–47.

Fatichi S, Ivanov VY, Caporali E. Simulation of future climate scenarios with a weather generator. Advances in Water Resources 2011;34(4):448–67.

Flato G, Marotzke J, Abiodun B, Braconnot P, Chou SC, Collins WJ, Cox P, Driouech F, Emori S, Eyring V. Evaluation of climate models. in: climate change 2013: the physical science basis. contribution of working group i to the fifth assessment report of the intergovernmental panel on climate change. Climate Change 2013 2013;5:741–866.

Forsythe N, Fowler H, Blenkinsop S, Burton A, Kilsby C, Archer D, Harpham C, Hashmi M. Application of a stochastic weather generator to assess climate change impacts in a semi-arid climate: The upper indus basin. Journal of Hydrology 2014;517:1019–34.

Fowler H, Blenkinsop S, Tebaldi C. Linking climate change modelling to impacts studies: recent advances in downscaling techniques for hydrological modelling. International Journal of Climatology 2007;27(12):1547–78.

Fowler H, Kilsby C, O'Connell P. A stochastic rainfall model for the assessment of regional water resource systems under changed climatic condition. Hydrology and Earth System Sciences Discussions 2000;4(2):263–81.

Fowler H, Kilsby C, O'connell P, Burton A. A weather-type conditioned multi-site stochastic rainfall model for the generation of scenarios of climatic variability and change. Journal of Hydrology 2005;308(1):50–66.

Francipane A, Fatichi S, Ivanov VY, Noto LV. Stochastic assessment of climate impacts on hydrology and geomorphology of semiarid headwater basins using a physically based model. Journal of Geophysical Research: Earth Surface 2015;120(3):507–33.

Fujibe F. Clausius–clapeyron-like relationship in multidecadal changes of extreme short-term precipitation and temperature in japan. Atmospheric Science Letters 2013;14(3):127–32.

Goderniaux P, Brouyere S, Blenkinsop S, Burton A, Fowler HJ, Orban P, Dassargues A. Modeling climate change impacts on groundwater resources using transient stochastic climatic scenarios. Water Resources Research 2011;47(12).

Goodess CM, Palutikof JP. Development of daily rainfall scenarios for southeast spain using a circulation-type approach to downscaling. International Journal of Climatology 1998;18(10):1051–83.

Gyasi-Agyei Y. Copula-based daily rainfall disaggregation model. Water Resources Research 2011;47:W07535.

Hardwick Jones R, Westra S, Sharma A. Observed relationships between extreme sub-daily precipitation, surface temperature, and relative humidity. Geophysical Research Letters 2010;37(22).

Hay LE, McCabe GJ, Wolock DM, Ayers MA. Use of weather types to disaggregate general-circulation model predictions. Journal of Geophysical Research-Atmospheres 1992;97(D3):2781–90.

Honti M, Scheidegger A, Stamm C. The importance of hydrological uncertainty assessment methods in climate change impact studies. Hydrology and Earth System Sciences 2014;18(8):3301.

Hulme M, Jenkins GJ, Lu X, Turnpenny JR, Mitchell TD, Jones RG, Lowe J, Murphy JM, Hassell D, Boorman P, McDonald R, Hill S. Climate Change Scenarios for the United Kingdom: The UKCIP02 Scientific Report. Technical Report; Tyndall Centre for Climate Change Research. School of Environmental Sciences, University of East Anglia, Norwich, UK; 2002.

Kaczmarska J, Isham V, Onof C. Point process models for fine-resolution rainfall. Hydrological Sciences Journal 2014;59(11):1972–91.

Kaczmarska JM, Isham VS, Northrop P. Local generalised method of moments: an application to point process-based rainfall models. Environmetrics 2015;26(4):312–25.

Kalnay E, Kanamitsu M, Kistler R, Collins W, Deaven D, Gandin L, Iredell M, Saha S, White G, Woollen J, Zhu Y, Chelliah M, Ebisuzaki W, Higgins W, Janowiak J, Mo KC, Ropelewski C, Wang J, Leetmaa A, Reynolds R, Jenne R, Joseph D. The ncep/ncar 40-year reanalysis project. Bulletin of the American Meteorological Society 1996;77(3):437–72.

Khazaei MR, Zahabiyoun B, Saghafian B. Assessment of climate change impact on floods using weather generator and continuous rainfall-runoff model. International Journal of Climatology 2012;32(13):1997–2006.

Kilsby C, Jones P, Burton A, Ford A, Fowler H, Harpham C, James P, Smith A, Wilby R. A daily weather generator for use in climate change studies. Environmental Modelling & Software 2007;22(12):1705–19.

Koutsoyiannis D, Onof C. Rainfall disaggregation using adjusting procedures on a poisson cluster model. Journal of Hydrology 2001;246(1):109–22.

Lenderink G, Attema J. A simple scaling approach to produce climate scenarios of local precipitation extremes for the netherlands. Environmental Research Letters 2015;10(8):085001.

Liuzzo L, Noto LV, Arnone E, Caracciolo D, Loggia GL. Modifications in water resources availability under climate changes: a case study in a sicilian basin. Water Resources Management 2015;29(4):1117–35.

Manning L, Hall J, Fowler H, Kilsby C, Tebaldi C. Using probabilistic climate change information from a multimodel ensemble for water resources assessment. Water Resources Research 2009;45(11).

Maraun D, Rust HW, Osborn TJ. Synoptic airflow and uk daily precipitation extremes. Extremes 2010a;13(2):133–53.

Maraun D, Wetterhall F, Ireson AM, Chandler RE, Kendon EJ, Widmann M, Brienen S, Rust HW, Sauter T, Themessl M, Venema VKC, Chun KP, Goodess CM, Jones RG, Onof C, Vrac M, Thiele-Eich I. Precipitation downscaling under climate change: Recent developments to bridge the gap between dynamical models and the end user. Reviews of Geophysics 2010b;48:RG3003.

Mehrotra R, Sharma A. Development and application of a multisite rainfall stochastic downscaling framework for climate change impact assessment. Water Resources Research 2010;46(7).

Molnar P, Fatichi S, Gaál L, Szolgay J, Burlando P. Storm type effects on super clausius-clapeyron scaling of intense rainstorm properties with air temperature. Hydrology and Earth System Sciences 2015;19(4):1753–66.

Moss RH, Edmonds JA, Hibbard KA, Manning MR, Rose SK, van Vuuren DP, Carter TR, Emori S, Kainuma M, Kram T, Meehl GA, Mitchell JFB, Nakicenovic N, Riahi K, Smith SJ, Stouffer RJ, Thomson AM, Weyant JP, Wilbanks TJ. The next generation of scenarios for climate change research and assessment. Nature 2010;463(7282):747–56.

Murphy JM, Sexton DMH, Jenkins GJ, Boorman PM, Booth BBB, Brown CC, Clark RT, Collins M, Harris GR, Kendon EJ, Betts RA, Brown SJ, Howard TP, Humphrey KA, McCarthy MP, McDonald RE, Stephens A, Wallace C, Warren R, Wilby R, Wood RA. UK Climate Projections Science Report: Climate change projections. Technical Report; Met Office Hadley Centre, Exeter; 2009.

Onof C, Arnbjerg-Nielsen K. Quantification of anticipated future changes in high resolution design rainfall for urban areas. Atmospheric Research 2009;92(3):350–63.

Pachauri RK, Allen MR, Barros VR, Broome J, Cramer W, Christ R, Church JA, Clarke L, Dahe Q, Dasgupta P. Climate change 2014: synthesis report. Contribution of Working Groups I, II and III to the fifth assessment report of the Intergovernmental Panel on Climate Change. Geneva, Switzerland: IPCC, 2014.

Paschalis A, Molnar P, Fatichi S, Burlando P. A stochastic model for high-resolution space-time precipitation simulation. Water Resources Research 2013;49(12):8400–17.

Peleg N, Fatichi S, Paschalis A, Molnar P, Burlando P. An advanced stochastic weather generator for simulating 2-d high-resolution climate variables. Journal of Advances in Modeling Earth Systems 2017;9(3):1595–627.

Pumo D, Arnone E, Francipane A, Caracciolo D, Noto L. Potential implications of climate change and urbanization on watershed hydrology. Journal of Hydrology 2017;554:80–99.

Qian B, Corte-Real J, Xu H. Multisite stochastic weather models for impact studies. International Journal of Climatology 2002;22(11):1377–97.

Rodriguez-Iturbe I, Cox D, Isham V. Some models for rainfall based on stochastic point processes. Proceedings of the Royal Society of LondonAMathematical and Physical Sciences 1987;410(1839):269–88.

Rodriguez-Iturbe I, Cox D, Isham V. A point process model for rainfall: further developments. Proceedings of the Royal Society of LondonAMathematical and Physical Sciences 1988;417(1853):283–98.

Schmitt FG. Continuous multifractal models with zero values: a continuous-multifractal model. Journal of Statistical Mechanics: Theory and Experiment 2014;2014(2):P02008.

Shaw SB, Royem AA, Riha SJ. The relationship between extreme hourly precipitation and surface temperature in different hydroclimatic regions of the united states. Journal of Hydrometeorology 2011;12(2):319–25.

Srikanthan R, McMahon T. Stochastic generation of annual, monthly and daily climate data: A review. Hydrology and Earth System Sciences Discussions 2001;5(4):653–70.

Sørup HJD, Christensen OB, Arnbjerg-Nielsen K, Mikkelsen PS. Downscaling future precipitation extremes to urban hydrology scales using a spatio-temporal neyman–scott weather generator. Hydrology and Earth System Sciences 2016;20(4):1387–403.

Sørup HJD, Georgiadis S, Gregersen IB, Arnbjerg-Nielsen K. Formulating and testing a method for perturbing precipitation time series to reflect anticipated climatic changes. Hydrology and Earth System Sciences 2017;21(1):345.

Stocker TF, Qin D, Plattner GK, Alexander LV, Allen SK, Bindoff NL, Bréon FM, Church JA, Cubasch U, Emori S, Forster P, Friedlingstein P, Gillett N, Gregory JM, Hartmann DL, Jansen E, Kirtman B, Knutti R, Kumar KK, Lemke P, Marotzke J, Masson-Delmotte V, Meehl GA, Mokhov II, Piao S, Ramaswamy V, Randall D, Rhein M, Rojas M, Sabine C, Shindell D,

Talley LD, Vaughan DG, Xie SP. Technical summary; Cambridge, United Kingdom and New York, NY, USA: Cambridge University Press. Climate Change 2013: The Physical Science Basis. Contribution of Working Group I to the Fifth Assessment Report of the Intergovernmental Panel on Climate Change. p. 33–115.

Sunyer M, Gregersen IB, Rosbjerg D, Madsen H, Luchner J, Arnbjerg-Nielsen K. Comparison of different statistical downscaling methods to estimate changes in hourly extreme precipitation using rcm projections from ensembles. International Journal of Climatology 2015;35(9):2528–39.

Sunyer M, Madsen H. A comparison of three weather generators for extreme rainfall simulation in climate change impact studies. In: 8th International Workshop on Precipitation in Urban Areas. 2009. p. 10–3.

Sunyer M, Madsen H, Ang P. A comparison of different regional climate models and statistical downscaling methods for extreme rainfall estimation under climate change. Atmospheric Research 2012;103:119–28.

Taylor KE, Stouffer RJ, Meehl GA. An overview of cmip5 and the experiment design. Bulletin of the American Meteorological Society 2012;93(4):485–98.

Thorndahl S, Andersen AK, Larsen AB. Event-based stochastic point rainfall resampling for statistical replication and climate projection of historical rainfall series. Hydrology and Earth System Sciences 2017;21(9):4433.

Trenberth KE, Dai A, Rasmussen RM, Parsons DB. The changing character of precipitation. Bulletin of the American Meteorological Society 2003;84(9):1205–17.

Trigo R, DaCamara C. Circulation weather types and their influence on the precipitation regime in portugal. International Journal of Climatology 2000;20(13):1559–81.

Utsumi N, Seto S, Kanae S, Maeda EE, Oki T. Does higher surface temperature intensify extreme precipitation? Geophysical Research Letters 2011;38(16):L16708. doi:10.1029/2011GL048426.

Verrier S, Mallet C, Barthes L. Multiscaling properties of rain in the time domain, taking into account rain support biases. Journal of Geophysical Research-Atmospheres 2011;116:D20119.

Vuuren DPV, Edmonds J, Kainuma M, Riahi K, Thomson A, Hibbard K, Hurtt GC, Kram T, Krey V, Lamarque JF. The representative concentration pathways: an overview. Climatic Change 2011;109(1-2):5.

Wasko C, Sharma A. Continuous rainfall generation for a warmer climate using observed temperature sensitivities. Journal of Hydrology 2017;544:575–90.

Westra S, Alexander LV, Zwiers FW. Global increasing trends in annual maximum daily precipitation. Journal of Climate 2013;26(11):3904–18.

Westra S, Fowler H, Evans J, Alexander L, Berg P, Johnson F, Kendon E, Lenderink G, Roberts N. Future changes to the intensity and frequency of short-duration extreme rainfall. Reviews of Geophysics 2014;52(3):522–55.

Willems P, Arnbjerg-Nielsen K, Olsson J, Nguyen V. Climate change impact assessment on urban rainfall extremes and urban drainage: Methods and shortcomings. Atmospheric Research 2012;103:106–18.

Yusop Z, Nasir H, Yusof F. Disaggregation of daily rainfall data using bartlett lewis rectangular pulse model: a case study in central peninsular malaysia. Environmental earth sciences 2014;71(8):3627–40.